Evaluating the performance of ground motion models for an intraplate earthquake using Bayesian inference and chimney fragility curves: 2021 Mw 5.9 Woods Point earthquake, Victoria, Australia

James La Greca[a], Mark Quigley[a], Jerry Vaculik[b], Peter Rayner[a], Trevor Allen[c]

Email: james.lagreca@student.unimelb.edu.au

Author Affiliation

[a]School of Geography, Earth, and Atmospheric Sciences, University of Melbourne, Parkville, Victoria, Australia

[b]School of Civil, Environmental and Mining Engineering, University of Adelaide, Adelaide, South Australia, Australia

[c]Geoscience Australia, GPO Box 378, Canberra, ACT, Australia

This is a non-peer reviewed preprint submitted to EarthArXiv.

This manuscript has been submitted to Earthquake Spectra for peer review.

Twitter: James_LaGreca

Abstract

The 22 September 2021 (AEST) M_W 5.9 Woods Point earthquake occurred in an intraplate setting (Victoria, southeastern Australia) approximately 130 km ENE of the central business district of Melbourne (pop. ~5.15 million). A lack of seismic instrumentation and low population density in the epicentral region resulted in a dearth of near-source instrumental and "felt" report intensity data. To evaluate the relative performance of ground motion models (GMMs) used in seismic hazard analysis for the region, we first surveyed unreinforced masonry chimneys following the earthquake to establish damage states and develop fragility functions. Using Bayesian inference and including pre-earthquake GMM rankings as Bayesian priors, we evaluate the relative performance of GMMs in predicting chimney observations for different fragility functions and seismic velocity profiles. GMM relative performance in the near-field of the Woods Point earthquake is generally consistent with pre-earthquake expert elicitation derived GMM rankings, although individual GMM weightings vary significantly. Consideration could be given to refining the weightings of GMMs in future national seismic hazard models for Australia. GMMs used within the NSHA18 for southeast Australia outperform non-NSHA18 GMMs with Allen (2012), Atkinson and Boore (2006), and Chiou and Youngs (2008) the highest ranking NSHA18 GMMs at a Vs30 of 1100 m/s.

Introduction

Ground-motion models (GMMs) are a key element of a probabilistic seismic hazard analysis (PSHA) (Bommer et al., 2010). In stable continental regions (SCRs) where moderate-to-large earthquakes are infrequent and the spatial density of seismic networks is low, instrumental strong ground motion data may be rare, particularly in near-source areas (within at <10-30 km epicentral distances). This can complicate objective analysis of GMM parameters and performance in predicting ground shaking intensities and distributions (Leonard et al., 2014).

In Australia, development of the National Seismic Hazard Assessment (NSHA) is led by the nation's public sector geoscience advisor, Geoscience Australia (GA). The NSHA 2018 (Allen et al., 2020) used an expert elicitation process (EEP) to estimate respective weightings of GMMs used to develop the national seismic hazard model (Griffin et al, 2018; Griffin et al., 2020). An important aspect of GMM evaluation is comparison of instrumentally-recorded ground motions with theoretical outputs from the GMMs to calculate the fit and relative ranks of potential models (Ghasemi and Allen, 2018). Seismometer coverage in Australia is sparse and this results in a lack of diverse GMMs specifically curated for the Australian continent (Allen, 2012). Three GMMs are commonly used in seismic hazard assessments and are developed specifically for use in Australia: Allen (2012), Somerville et al. (2009) cratonic, and Somerville et al. (2009) non-cratonic. Other models used in NSHA 2018 have been adapted from California (Boore et al., 2014), Europe (Chiou and Youngs, 2008; Chiou and Youngs, 2014) and Central Eastern US (Atkinson and Boore, 2006). In previous editions of the NSHA, two other GMMs curated for Australia were used as candidates; Gaull et al., (1990) South East Australia, and Gaull et al., (1990) Western Australia. These models were removed in NSHA18 due to their relatively poor performance against newer and adapted GMMs largely due to the model's local magnitude (M_L) to moment magnitude (M_W) conversion. Future editions of the NSHA are considering the adaption of the Next Generation Attenuation for Central and Eastern North America (NGA-East (Goulet et al., 2021)) as a GMM candidate.

Unreinforced masonry (URM) chimneys are amongst the most damage-prone components across any building class when subjected to earthquake ground motion (Krawinkler et al., 2012; Maison and McDonald, 2018; Moon et al., 2014). Modelling of masonry chimney fragility curves can provide a prediction of seismic vulnerability and damage in the event of an earthquake as an expression of peak ground acceleration (PGA). Fragility curves that define seismic vulnerability for chimneys surveyed after an earthquake can be used as a proxy to determine intensity of shaking. Fragility curves define a cumulative distribution function with respect to PGA. The intersection between the fragility curve and the output of a GMM defines the probability of damage. In this paper, Bayesian modelling is used to evaluate relative likelihoods of GMMs dependant on their PGA outputs for respective chimney fragility curves.

Bayes' theorem (Bayes, 1764; Joyce, 2003) states that one can calculate the posterior probability using a prior probability and likelihood function. If the likelihood of a calculated PGA (derived from a GMM) to cause damage to a chimney is known, the likelihood a GMM is correct given the observational data can be calculated. Therefore, using Bayes theorem and residential chimney fragility functions, the likelihood that a ground motion model represents the expected damage outcome of a set of chimneys after an earthquake can be deduced.

This paper aims to answer the following questions:

1. Using earthquake damage of chimneys and their respective fragility curves as a proxy for seismic ground motions at near-source locations, what is the relative performance of commonly used GMMs in terms of their ability to predict the chimney damage observations?

2. How do the relative weightings of GMMs established from a chimney analysis using a Bayesian approach compare with pre-Woods Point earthquake EEP weightings of GMMs?

This paper outlines a method to evaluate the relative performance of GMMs in response to an earthquake where no near source instrumental seismic data is present. Two chimney fragility curve models (M1: Maison and McDonald, (2018); M2: Fragility Curves computed by this study based on Vaculik and Griffith, 2019) and median GMM PGA curves are used as inputs into a Bayesian analysis. A Bayesian approach is used to determine which GMM best matches the chimney damage observations from the Woods Point earthquake.

2021 MW 5.9 Woods Point earthquake

At 9:15 am on the 22nd of September 2021 (AEST), a M_W 5.9 earthquake occurred in southeast Australia within the Southeast Seismic Zone, approximately 130 km ENE of Melbourne's CBD (Figure 1). This intraplate event was the largest earthquake in the state of Victoria since European record keeping began in the early 1800s (McCue, 2015). The epicentral region is sparsely populated; Woods Point (pop. 33), Jamieson (pop. 382), and Licola (pop. 11) are the three settlements nearest the epicentre (2021 Census). The mainshock occurred in the Victorian Highlands, approximately 13 km ENE from Woods Point. Three epicentral locations have been published;

GA: -37.490, 146.35, depth of 10 km;

Seismology Research Centre (SRC): -37.506, 146.402, depth of 12.7 km;

United States Geological Survey (USGS): -37.486, 146.347 (± 4.8 km), depth of 12.0 km (± 1.7 km).

The location published by SRC is preferred as it uses additional data from a commercial seismometer network that is not used in the GA and USGS analyses. Epicentral locations are identified as one of the many inputs that contribute to epistemic uncertainty in GMMs. Focal mechanisms published from the main shock delineate a steep dipping (83-84°) strike-slip fault with a strike of 172° (GA)(west-dipping) or 351° (USGS)(east-dipping). Aftershock locations and clusters determined by the SRC delineate an ~8 km long NNW-striking plane with a ~85° dip that Quigley et al., (2021) and Quigley and La Greca, (2021) attribute as the source fault for the Woods Point mainshock. We use the USGS focal mechanism as the preferred fault for this analysis. The nearest seismometer is a short period passive sensor, located 35 km from the epicentre at Thompson Reservoir (TOT) (Figure 1). Earthquake waveforms at TOT clipped under the Woods Point earthquake ground motions. Preliminary observations of ground motions (Hoult et al., 2021) omit TOT data from analysis.

Geoscience Australia used four equally weighted GMMs (AB06, SEA09NC, A12, and BEA13) and a 0-30 m depth-time averaged shear-wave velocity model (V_{S30}) based on the Australian

Seismic Site Conditions Map (McPherson, 2017) to produce PGA contour plots for the Woods Point earthquake (Figure 1) (Allen et al., 2019a; Allen et al., 2021). These PGA contours are informed by the 'ShakeMap' system in which GMMs, ground motion amplification based on topographic slope, and 'felt' reports into a seismic intensity are combined to create a map of seismic intensity (Allen et al., 2019b; Wald et al., 2010). Estimated PGAs within the epicentral region are ~0.2 g. PGAs in Melbourne (Figure 1) range from 0.02 to 0.05 g.

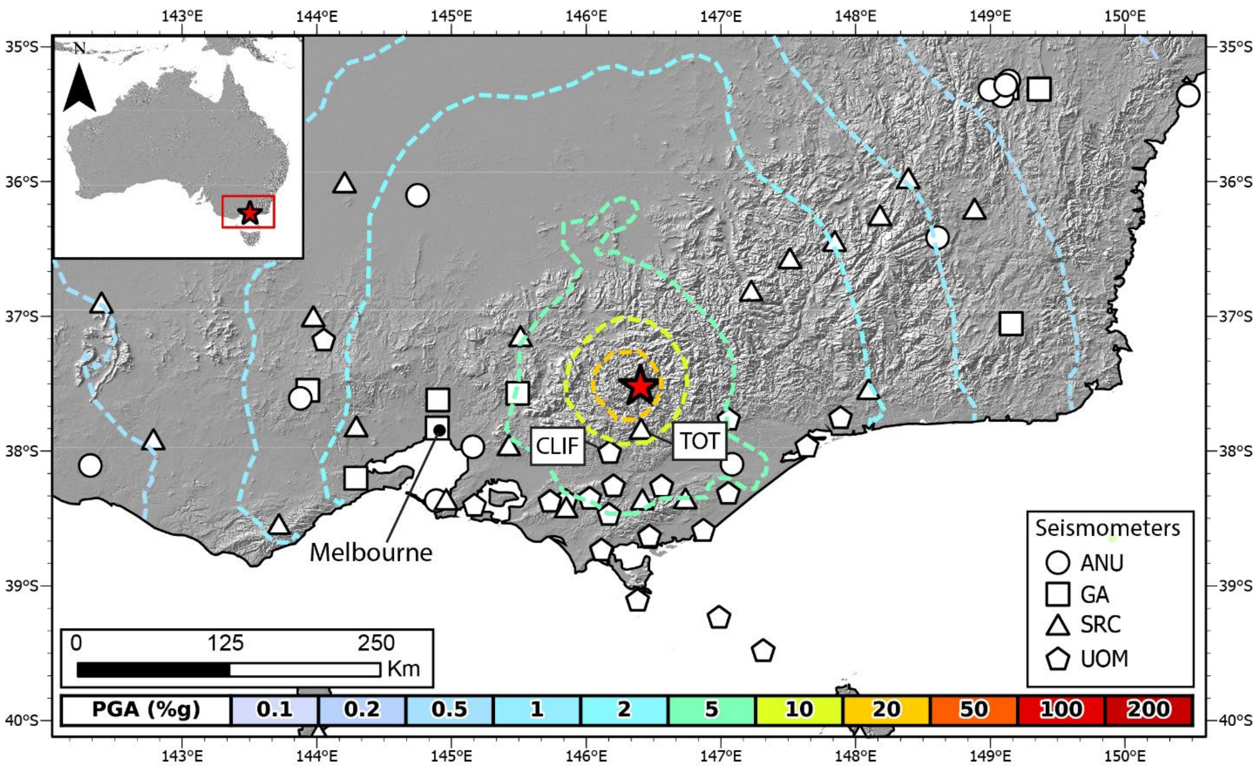

Figure 1: Map of seismometer locations in southeastern Victoria and GA PGA contours.

Instrumentally recorded spectral accelerations (SA) of the Woods Point earthquake are primarily within the range of, or exceed, GMM-predicted median values across a range of periods (Figure 2.) (Hoult et al., 2021a).

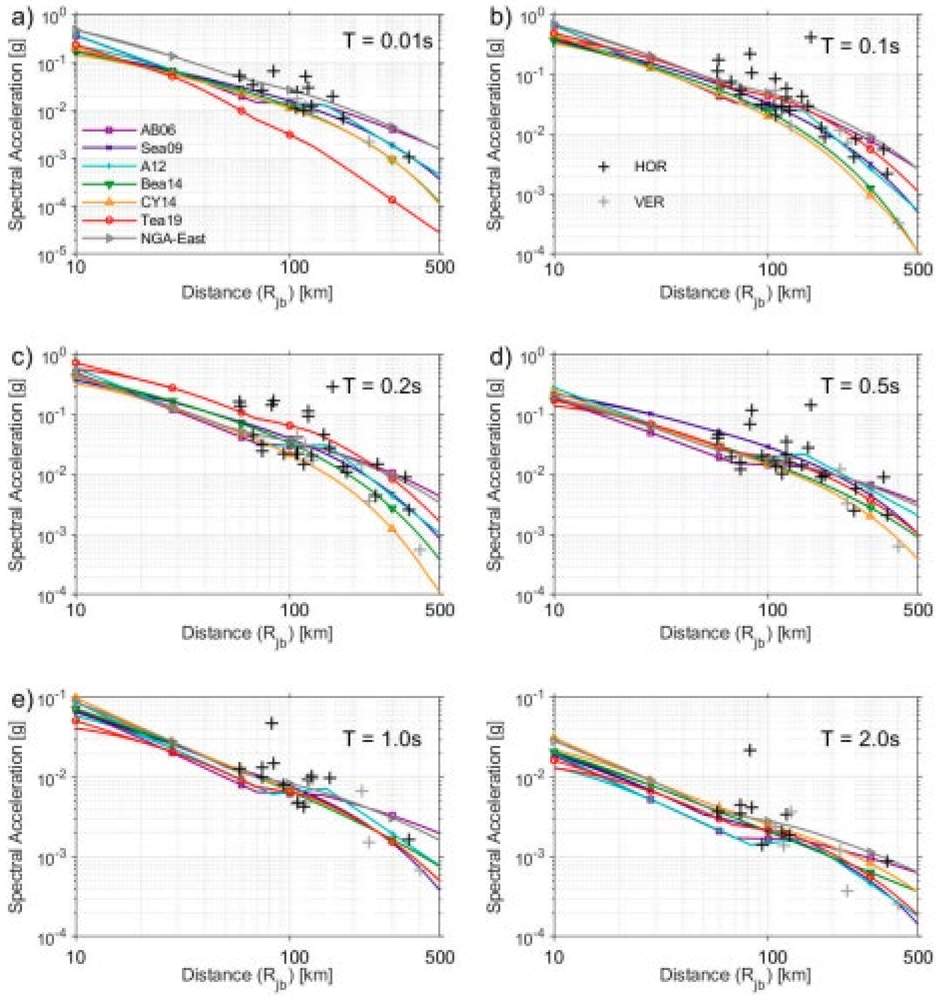

Figure 2: Spectral Accelerations from GMMS for Woods Point EQ (Hoult et al., 2021a).

The absence of observational data at epicentral distances less than 60 km precludes comparison of GMM predictions against observations in the near source region. It is likely that some instrumental data has been recorded from locations with Vs30 greater than the Vs30 used to construct the GMMs. The assumption is these sites have a Vs30 of 760 m/s which Hoult et al., 2021a states is unlikely to be the case. This, and other source to site effects likely contribute to variability between observations and predictions in Figure 2. Given the absence of near source instruments, we do not attempt to model near source SAs for the Woods Point earthquake.

Modified Mercalli Intensity (MMI) data derived from nearly 43,000 “felt” reports exhibit large spatial density variations. The sparsely populated epicentre area contains few observations (Figure

3). The majority of reports are derived at epicentral distances of ~130 km, in and around Greater Melbourne – the highest population density in Victoria.

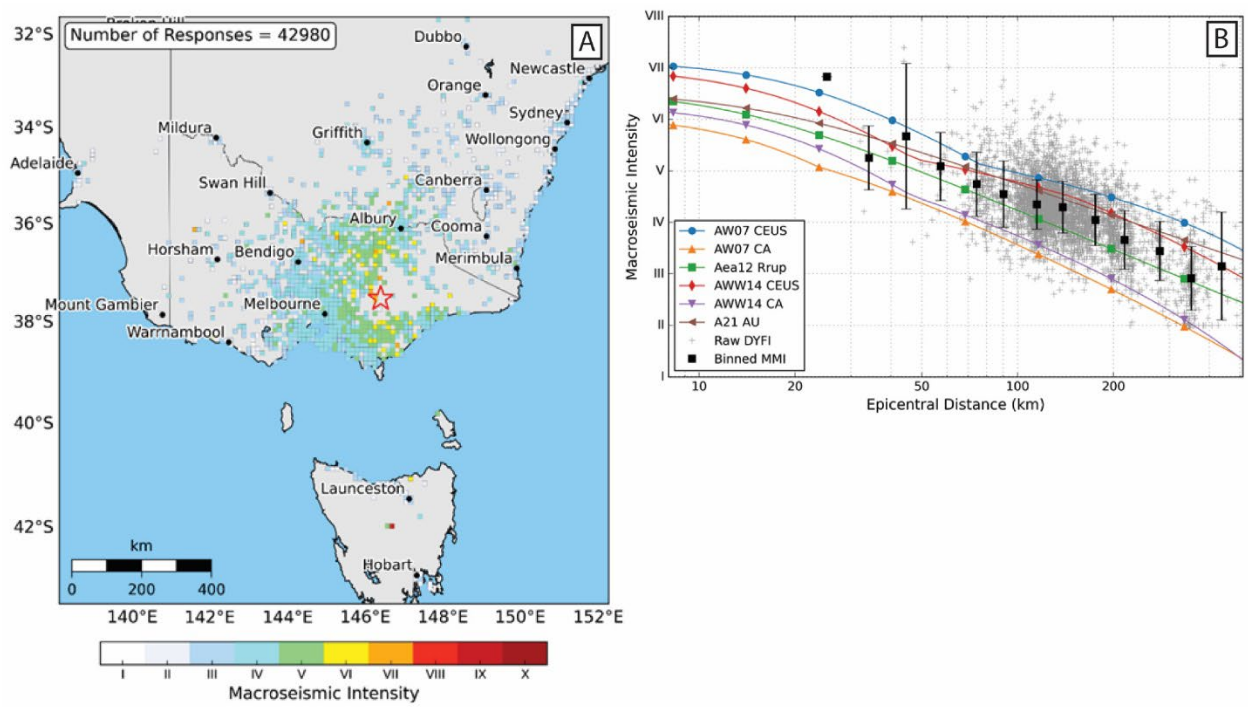

Figure 3A: "Felt" grid estimated from some 43,000 "felt" reports submitted to Geoscience Australia following the 22 September 2021 Woods Point earthquake. Figure 3B: MMI attenuation model equations of the Mw 5.9 Woods Point earthquake with one sigma confidence using MMI GMMs

Figure 3A and Figure 3B exhibit paucity of near-source information that could be used to assess attenuation relationships and reveal substantive variability that could reflect source and site effects on ground motion intensities and highlight variations in the uncertainty of using proxies to derive MMI estimates (e.g., differing building fragilities).

Woods Point Reconnaissance Survey

A reconnaissance field survey of environmental and infrastructure damage in the epicentral area commenced ~30 hours after the earthquake (23-27 September 2021) (Quigley and La Greca, 2021; La Greca and Quigley, 2021). Subsequent field surveys were undertaken on October 8-10 and 23-26. Field investigations enables us to identify 43 brick masonry and four stone chimneys (n = 47) including chimneys with damage (Figure 4). All chimneys were physically examined, precisely located, and photographed from multiple angles (Figure 5). Chimney width and heights were determined by brick counting on photographic images, using the average Australian brick size (76 mm high x 230 mm long x 110 mm wide), with exception of the four stone chimneys, where height was approximated using scaled photographs. Visual inspection of mortar in the field and on photographs enabled us to estimate mortar 'quality' and 'age' that formed an input in fragility analyses. This included up close investigation of the mortar, determining whether it was flaking and/or breaking apart. Mortar observations also enabled us to distinguish earthquake from pre-earthquake damage; e.g., if a chimney had small cracking in the mortar and/or bricks but had moss growing within the crack, it was interpreted to be pre-seismic deformation. All chimney data is presented in Appendix A and Appendix B. Of the total chimneys observed, five were determined to have collapsed in the earthquake or suffered extensive damage.

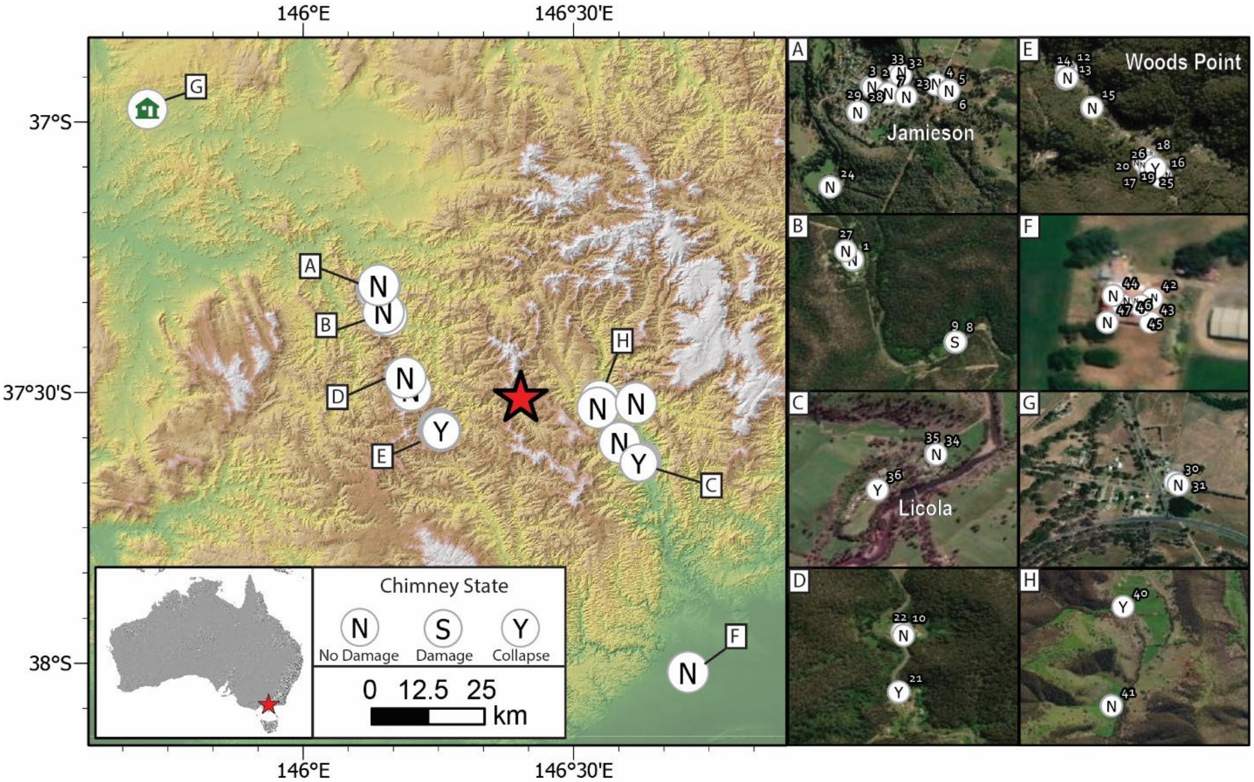

Figure 4: Map of Chimneys observed in the reconnaissance survey and their respective collapse state resultant from the Woods Point earthquake.

Figure 5: Photos of chimneys with various damage states post the Woods Point earthquake.

Methodology

Selection of GMMs and Vs30

A summarised schematic of the methodology is provided Figure 6. Text is used to describe the methodology section in the order outlined in the schematic. GMMs are used in this study, on the basis that they were used in the Australian NSHA18, previously a part of it, or being considered to be a candidate GMM. They include Allen (2012), Atkinson & Boore (2006), Boore et al. (2014), Chiou & Youngs SWISS1 (2008), Chiou & Youngs (2014), Somerville et al. non-cratonic (2009), Somerville et al. Yilgarn Craton (2009), Gaull et al. South East Australia (1990), Gaull et al. WA (1990), and NGA-E (Goulet et al., 2021). GMMs currently contributing to the NSHA18 can be seen in Table 1 with their respective expert elicitation weights. Integration distance is the GMM cut-off distance for earthquake sources.

Table 1: Final ground motion model weights applied in the NSHA18, modified from the GMC expert elicitation workshop (adapted from table 8 in Griffin et al., 2018)

Model Name	Tectonic Region Type	Intra-Region Weight	Reference	Integration Distance
Allen2012 (A12)	Non-Cratonic, Extended, Oceanic and Active Crust	0.208	Allen (2012)	400 km
AtkinsonBoore2006 (AB06)		0.138	Atkinson and Boore (2006)	
BooreEtAl2014 (BEA14)		0.166	Boore *et al.* (2014)	
ChiouYoungs2008SWISS01 (CY08)		0.153	Edwards *et al.* (2016)	
ChiouYoungs2014 (CY14)		0.130	Chiou and Youngs (2014)	
SomervilleEtAl2009NonCratonic (SEA09NC)		0.205	Somerville *et al.* (2009)	

The computation was run for five different V_{S30} values; 270, 400, 560, 760, 1100 (m/s) as the V_{S30} at each chimney site is unknown.

URM Chimney Fragility Models

The vulnerability of URM chimneys to earthquake ground motions was modelled by two alternate fragility models including that by Maison and McDonald (2018) and Vaculik and Griffith (2019). The output of both models is a set of analytical fragility curves that express the probability of a chimney reaching a particular damage state as a function of ground motion intensity in terms of the PGA. The more resilient a chimney is, the further the fragility curves will shift towards higher PGA values. These curves in turn serve as the input into the Bayesian analysis in the subsequent portion of this paper. The decision to consider two separate fragility models was made to improve the reliability of the Bayesian inference process given the inherent uncertainty in relating the expected damage states to ground motion intensity. PGA values are calculated using selected GMMs within the OpenQuake hazardlib software library at a distance equivalent to the source-to-site distance required by the GMM for each chimney on a range of site conditions (Pagani et al., 2014). These estimates were used to determine the probability of the chimney sustaining the degree of damage (or non-damage) that was observed. The Bayesian analysis represents the likelihood of each individual GMM to correctly predict the field-derived damage observations under the assumption that the fragility curve is representative of a 'chimney's' damage potential. Additionally, the Bayesian analysis considers and incorporates two prior inputs. A uniform prior which assumes there all GMMs have an equal weight before entering the Bayesian analysis and a NSHA18 prior approach, where the NSHA18 logic tree weights are applied into the Bayesian analysis. PGA values output by GMMs in this process do not consider aleatory variability and takes the assumptions that the median GMM value is the PGA at the site of the chimney.

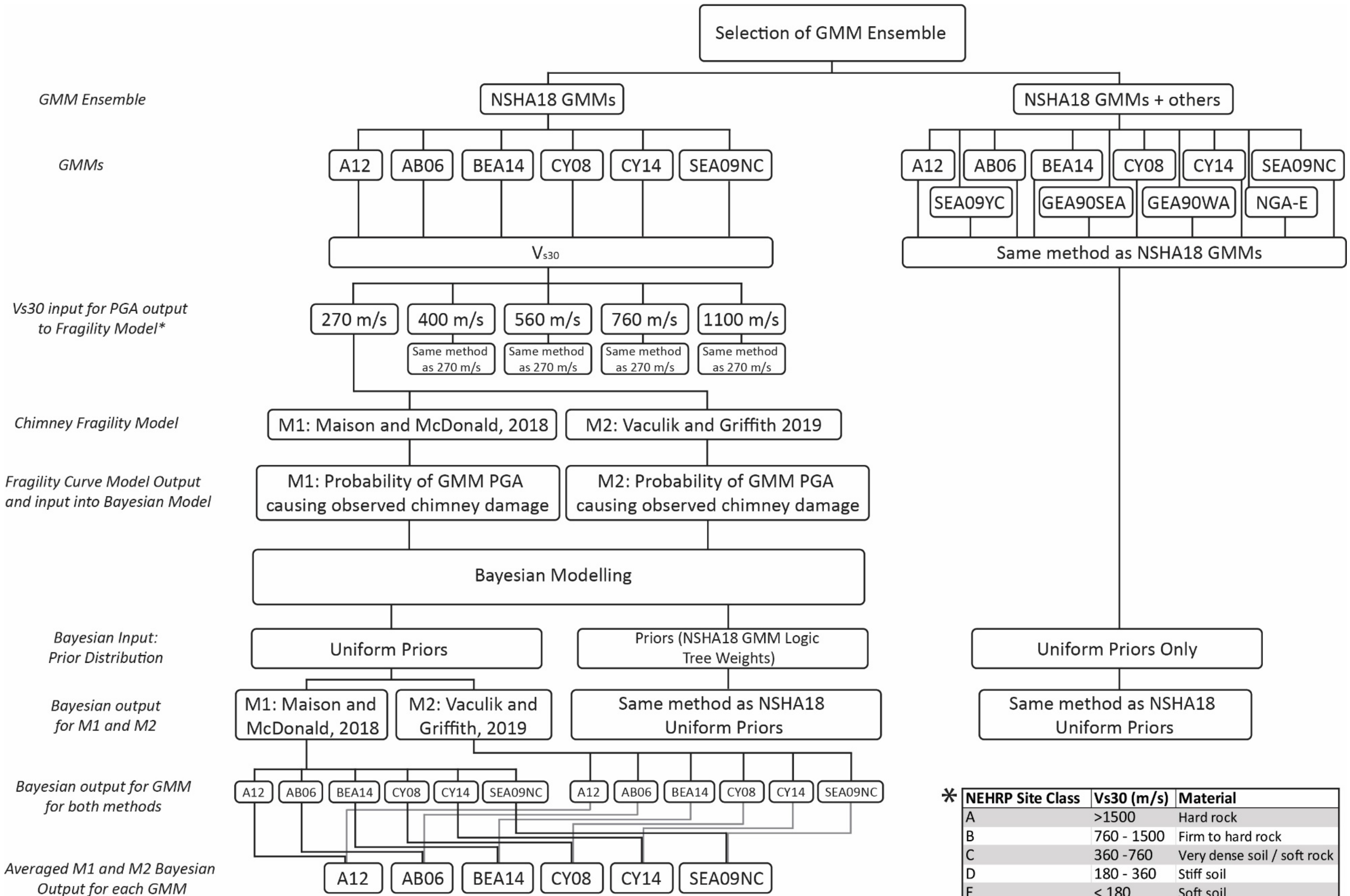

*

NEHRP Site Class	Vs30 (m/s)	Material
A	>1500	Hard rock
B	760 - 1500	Firm to hard rock
C	360 -760	Very dense soil / soft rock
D	180 - 360	Stiff soil
E	< 180	Soft soil
F	-	Soils requiring testing

Figure 6: Summary of methodology

Fragility Curve Method One: Maison and McDonald, 2018

The fragility curves of Maison and McDonald (2018) were determined using a single-degree-of-freedom computer model (Maison and McDonald, 2018). Fragility curves incorporate the effects of various site parameters including chimney height above roof, masonry flexural tensile strength, chimney section dimensions, vertical steel reinforcement, and chimney house anchorage strength. Damage functions for unreinforced masonry chimneys are expressed as a function of PGA, chimney height and expected masonry tensile strength for the chimneys part of this study can be seen in Figure 7A and Figure 7B.

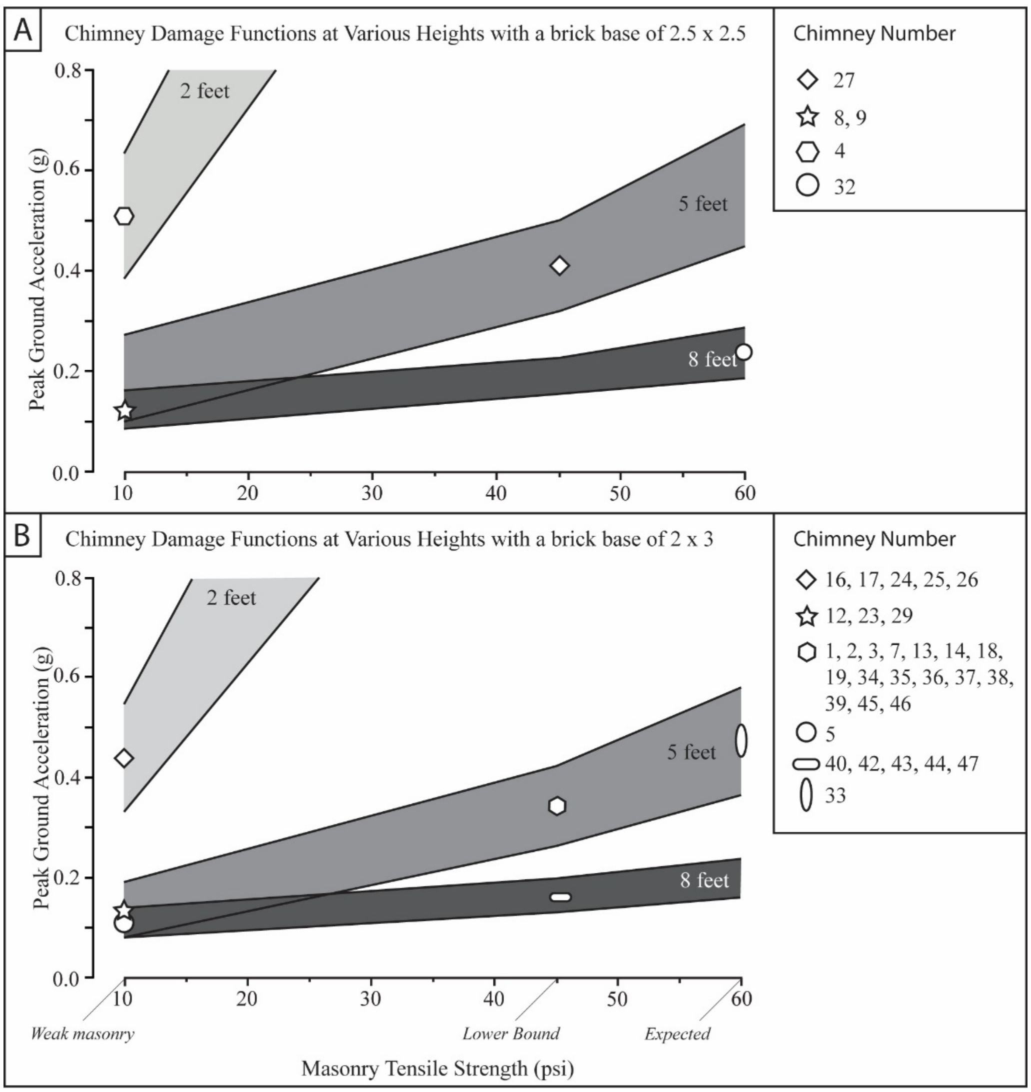

Figure 7: Damage functions for chimneys as outlined by Maison and McDonald (2018). Chimneys from reconnaissance survey plotted onto damage curve to obtain median value.

A select set of chimneys in the Woods Point epicentral region did not meet the brick base templates used in Maison and McDonald (2018). Maison and McDonald (2018) suggest that the shortest measurement of either the length or width of the chimney dictates the damage function (Figure 8). Therefore, in this study for a chimney to be included it must meet one only one measurement of the brick base outlined in Figure 7A and Figure 7B.

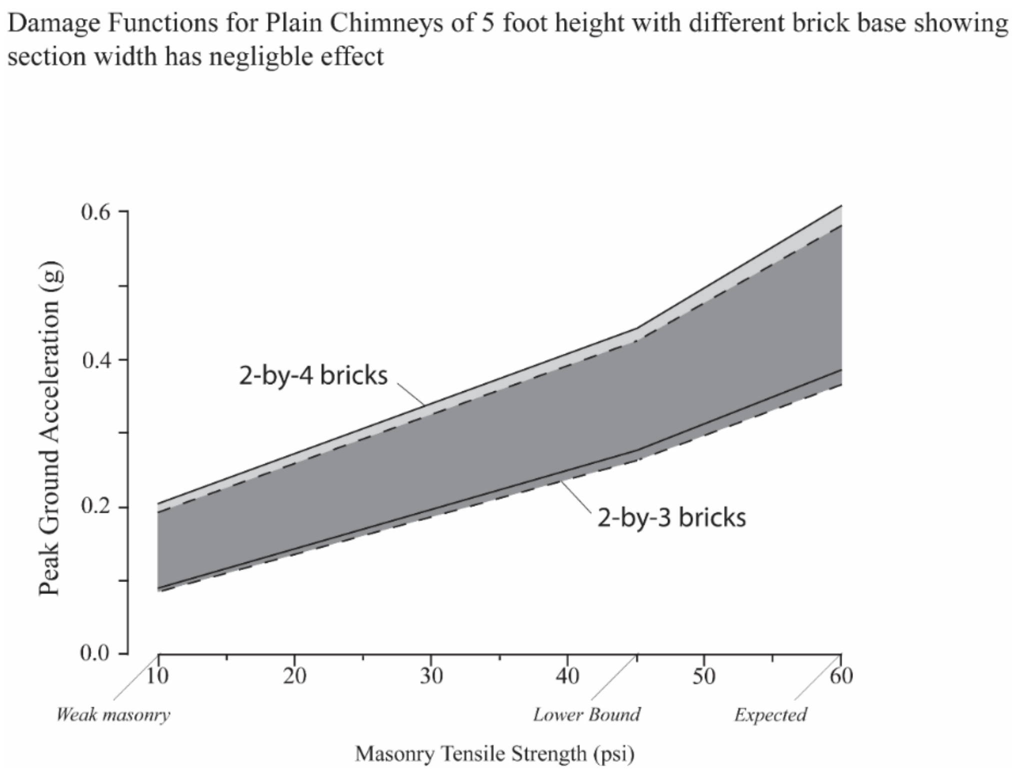

Figure 8: Damage function displaying difference of chimney section width (Maison and McDonald 2018).

This method still cannot account for all the chimneys surveyed in response to the Woods Point earthquake. Chimneys 6, 10 ,11, 15, 20, 21, 22, 30, 31, and 41 were not able to be assessed using this method. Specifically, chimney brick type (stone chimneys were omitted), height, and brick base were the three reasons a chimney would be omitted from method one if it could not meet the dimension set in Figure 7. All chimneys are evaluated in model 2 (see next section, Model 2).

The conversion of damage functions to a fragility curve can be made if the median value of the damage function is known paired with the beta value. The PGA value obtained from the median line in the damage functions represents the median (50%) value of the fragility curve. The beta value chosen then dictates the distribution of the fragility curve. This is used to incorporate uncertainty within the fragility curve. Uncertainty can come from material property, measurement uncertainties, and whether the fragility model actually captures chimney behaviours. Maison and McDonald (2018) state uncertainty can be varied and difficult to quantify, therefore suggest using a beta value of 0.6 as per US. FEMA P-58 Seismic Performance Assessment of Buildings, Methodology, and Implementation guidelines (FEMA, 2018).

Fragility Curve Generation Model Two: Vaculik and Griffith, 2019

The second fragility model follows the analytical approach described in Vaculik and Griffith (2019) which utilizes a two-step time-history analysis (THA). The first step is to perform a THA on the parent building with excitation by the ground motion, and by doing so, compute the motion at the top of the building. This motion is in turn used as the excitation in the second step, which involves undertaking a nonlinear THA of the chimney. The chimney's force-displacement behaviour was defined using a bilinear rule with a descending post-yield branch to represent rocking behaviour (Vaculik and Griffith, 2017). Unlike the Maison and McDonald approach, this model ignores any bond strength and assumes that the chimney's lateral load resistance is provided entirely from stabilization due to gravity. The force-displacement capacity of each chimney was constructed as a function of its geometry; that is, the height above the roof line and base width. In the case of rectangular chimneys (with unequal base widths), the shorter dimension was used. A factor of 0.9 was applied to the gross width of the chimney to account for deviation from idealized rigid behaviour, for example due to geometric imperfections and finite compressive strength.

Following the approach described in Vaculik and Griffith (2019), a set of five displacement-based damage levels were defined, ranging from D1 (first onset of cracking) to D5 (complete collapse). In order to align these with the observable damage levels in the field survey, these were condensed into three states: 1) no visible damage (damage $<$ D2), 2) visibly damaged but not collapsed (damage $\geq$ D2 but $<$ D4), and 3) collapsed (damage $\geq$ D4). Note that the onset of observable damage was set at D2 rather than D1, due to micro-cracking not being able to be visually assessed in the field.

This overall procedure was implemented within an incremental dynamic analysis using a suite of code-compatible (Standards Australia, 2018) ground motions, from which the median PGAs to reach different damage states were computed, thus resulting in a standalone set of fragility curves for each chimney. Further detail regarding the overall approach can be found in Vaculik and Griffith (2019).

As with the first model, a beta value of 0.6 was adopted for the dispersion of the fragility curves consistent with FEMA guidelines.

Plotting of Fragility Curves

Fragility curves were formulated in terms of the lognormal distribution, whose cumulative distribution function (CDF) can be expressed as:

$$F(x) = \Phi\left(\frac{\ln x - \mu}{\beta}\right) \quad (1)$$

where x is the PGA; Φ is the standard normal CDF operator; μ is the natural logarithm of the median PGA at each damage state; and β is the coefficient of variation (= standard deviation / mean, or alternately the standard deviation in log-space) (Lallemant et al., 2015), which was taken as 0.6 in both models.

Illustrative examples of fragility curves obtained using the respective models are shown in Figure 9 (see appendix A for all chimneys). These consider three chimneys:

- Chimney 17 – a stocky (~2 feet tall) chimney assumed to have weak bond (10 psi)
- Chimney 1 – a medium-slenderness (~5 feet tall) chimney assumed to have typical-strength bond (60 psi)
- Chimney 32 – a slender (~8 feet) tall chimney assumed to have normal-strength bond (60 psi)

It is seen that the solitary curves for model 1 coincide roughly with damage state D5 curve in model 2; and thus, the median PGA of the D4 curves in model 2 (delineating the collapse state in the implementation throughout this paper) are typically lower than the PGAs predicted by model 1.

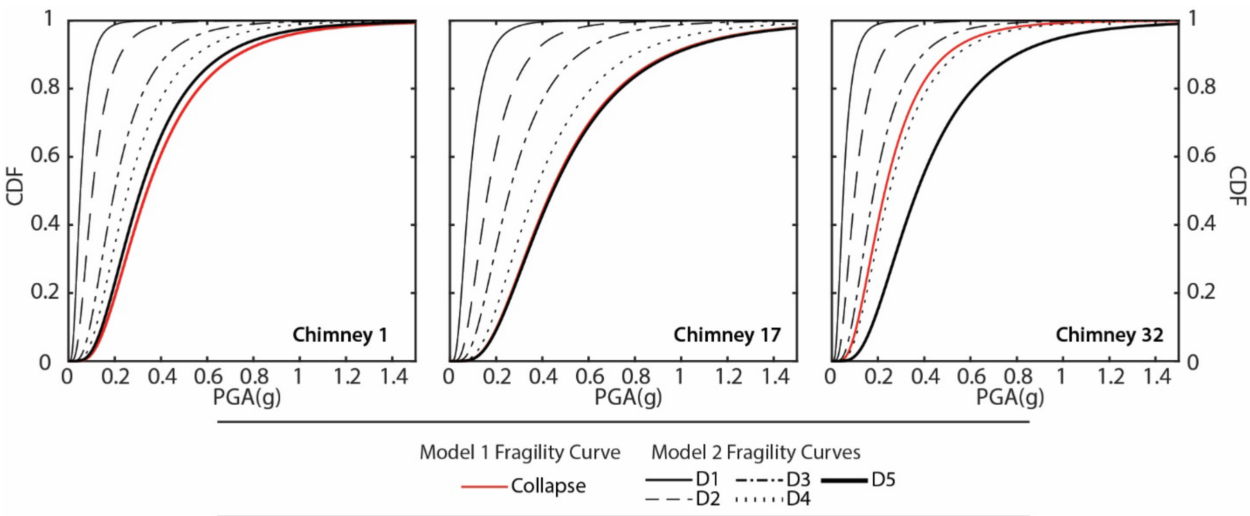

Figure 9: Examples of fragility curves from three different chimneys for both models of curve generation

Peak Ground Acceleration Calculation – OpenQuake

OpenQuake (https://platform.openquake.org/) was used to compute the expected peak ground accelerations at each chimney using the earthquake scenario function (Pagani et al. 2014). The OpenQuake-engine is a seismic hazard and risk modelling platform developed by the Global Earthquake Model (GEM) Foundation (Pagani et al., 2014). The software is developed within a rigorous, test-driven framework and is designed to be both modular and flexible.

Input Files

The earthquake rupture file was completed using the Seismology Research Centre (SRC) hypocentre and data from the Woods Point earthquake information sheet (Quigley et al., 2021) (Table 2)

Table 2: Rupture Inputs required for OpenQuake earthquake rupture

Woods Point earthquake OpenQuake inputs	
Mw	5.9
Rake	0
Hypocentre Longitude	146.402
Hypocentre Latitude	-37.506
Hypocentre Depth	12.7 km
Rupture Type	Simple Fault Rupture
Dip	85 Degrees
Upper Seismogenic Depth (km)	4
Lower Seismogenic Depth (km)	13
Fault Geometry	146.394, -37.5417 146.380, -37.470

The calculated PGA value from each GMM using OpenQuake for each chimney can then be compared to the respective fragility curves. Figure 10 shows an example of five chimneys displaying that the intersection point of the expected PGA and the fragility curve determines probability values inputs for the Bayesian model.

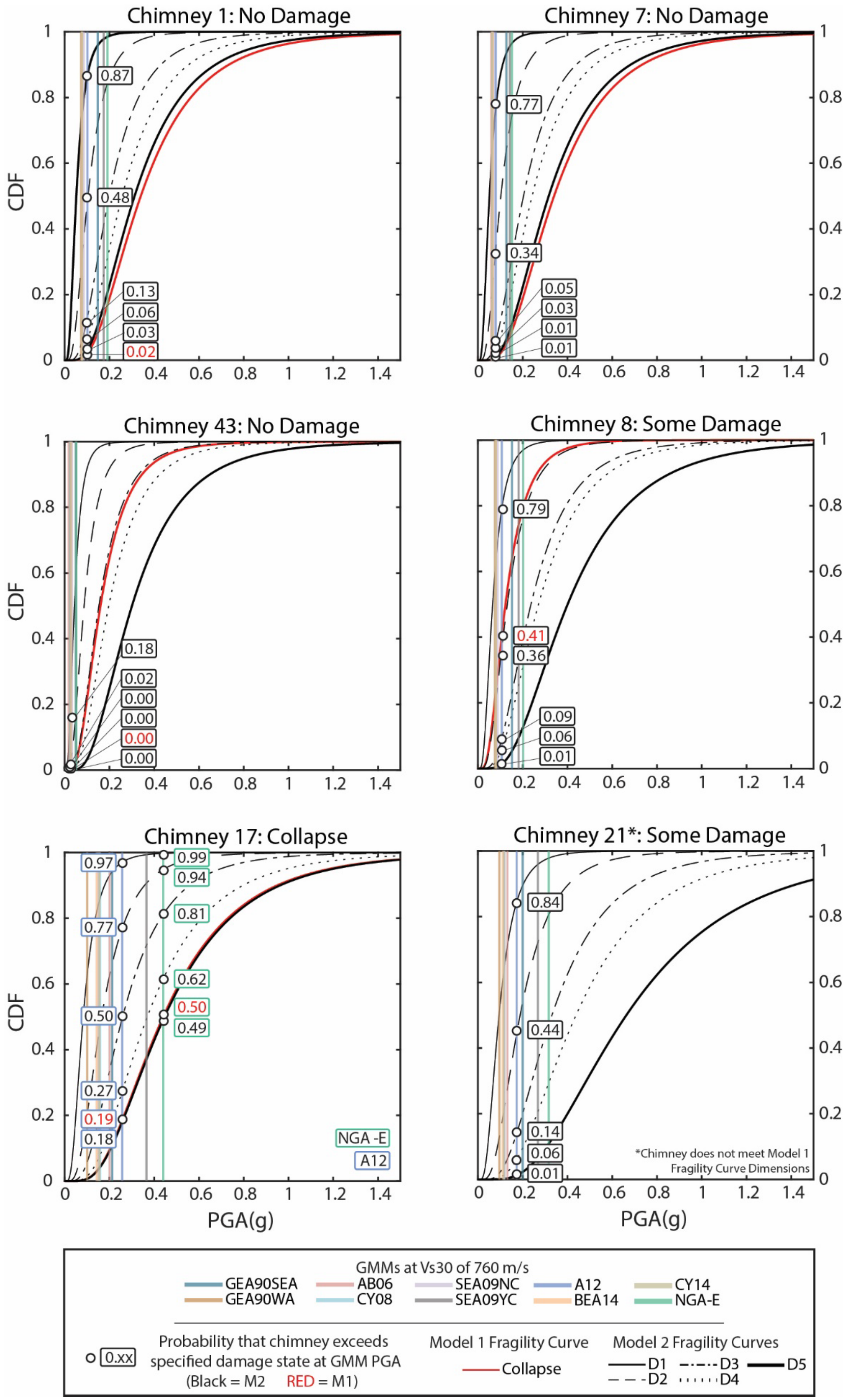

Chimney 1: No Damage
Chimney 7: No Damage
Chimney 43: No Damage
Chimney 8: Some Damage
Chimney 17: Collapse
Chimney 21*: Some Damage
CDF
PGA(g)
NGA -E
A12
*Chimney does not meet Model 1 Fragility Curve Dimensions
GMMs at Vs30 of 760 m/s
GEA90SEA
GEA90WA
AB06
CY08
SEA09NC
SEA09YC
A12
BEA14
CY14
NGA-E
Probability that chimney exceeds specified damage state at GMM PGA (Black = M2 RED = M1)
Model 1 Fragility Curve
Collapse
Model 2 Fragility Curves
D1
D2
D3
D4
D5

354

Figure 10: Selection of Chimney fragility curves with the expected PGA for each GMM and the respective probability the chimney exceeds each damage state. The intersection points of GMM A12 with the fragility is highlighted and presents the probability that the PGA estimated by A12 with cause the defined fragility damage state. Chimney 17 also has NGA-E highlighted to show variation in GMM outputs.

The PGA – fragility curve intersection point represents the probability the chimney will exceed a specified damage state at that PGA for each given GMM for six selected chimneys. Depending on the damage state of the chimney resulting from the earthquake, the probability of the observed can be determined through either taking the intersection CDF (if chimney had damage), or through subtracting the CDF from 1 (if the chimney had no damage). M1 (Maison and McDonald, 2018) uses a binary damage state for collapse or no collapse (red line in Figure 10). M2 (Vaculik and Griffith, 2019) uses five damage states to model chimney damage (black lines in Figure 10). For chimneys that had damage but did not collapse, the CDFs for the damage range were subtracted from one another. These probabilities of observed values were used as inputs in the Bayesian approach.

Bayesian Model

Bayesian modelling is a statistical approach based on Bayes' theorem taking knowledge from observed data to update a statistical model (van de Schoot et al., 2021). A prior distribution (background knowledge) can be informed by new observational data to establish a new posterior probability. Bayes' theorem states that one can calculate the posterior probability if the prior probability and the likelihood function is known. This approach will calculate the probability of a ground motion model (A) being true, given the likelihood of a chimney exceeding a damage state (B) in the result of an earthquake.

This can be expressed as:

$$P(A|B) = \frac{P(B|A) \cdot P(A)}{P(B)} \tag{2}$$

Where P(A|B) is the probability a ground motion model is true given event B (the posterior belief), P(B|A) is the probability chimneys will exceed a damage state given the expected ground motion output from a ground motion model (A) of observing our resulting based on chimney fragility curves. P(B) is the probability of each chimney reaching various damage states as outlined by their fragility curve and P(A) is the prior distribution of our ground motion model before the earthquake event. P(B|A) is determined through three different equations depending on the state of the chimney. As there are two methods of fragility curve generation, this analysis will examine the combination of these methods into a singular P(B|A) value.

Calculation of P(B|A)

M1

There are two states of chimneys in this method. Chimneys that have collapsed, and chimneys that have not. For chimneys that have collapsed, the fragility curve dictates the probability of the observed and therefore is represent as follows:

$$P1(B|A) = \prod \Phi\left(\frac{\ln x - \mu}{\beta}\right) \tag{3}$$

For chimneys that have not collapsed, one subtract the probability of collapse equals the probability of observed and is represented as follows.

$$P2(B|A) = \prod 1 - \Phi\left(\frac{\ln x - \mu}{\beta}\right) \qquad (4)$$

where x = specified PGA value for individual chimney
μ = Natural Log value of fragility curve median
β = beta value in fragility curve analysis
Φ is the standard normal CDF operator

To calculate P(B|A), it is the product of P1(A|B) and P2(A|B):

$$P(B|A) = P1(A|B) \cdot P2(A|B) \qquad (5)$$

M2

This method considers three damage states: undamaged, damaged and collapse (Table 3). Therefore, to calculate the P(B|A) for a given ground motion model that incorporates three chimney damage states, three equations are derived. The undamaged state is represented in equation (5). 'No damage' was interpreted as not exceeding a D-Level of 2, and therefore the median value (μ) is defined by the D2 curves in Appendix C for each chimney. Equation (6) defines P3(B|A). The second is for chimneys that have sustained damage, but not total collapse. This will be the probability the chimney would sustain a lower damage level then subtracting the probability the chimney would fail from the higher damage level. This will assume a level of damage greater than a D-Level of 2 but not greater than 4. This is equation (7) and defines P4(B|A). The third scenario is for chimneys that have failed. This will be the probability the chimney would fail at that damage state and represents the likelihood of damage at a minimum D-Level of 4. This is equation (8) and defines P5(B|A). These three calculations ultimately state the probability of the observed event and can be seen in Appendix D.

$$P3(B|A) = \prod 1 - \Phi\left(\frac{\ln x - (D2)\mu}{\beta}\right) \qquad (6)$$

$$P4(B|A) = \prod \Phi\left(\frac{\ln x - (D2)\mu}{\beta}\right) - \Phi\left(\frac{\ln x - (D4)\mu}{\beta}\right) \qquad (7)$$

$$P5(B|A) = \prod \Phi\left(\frac{\ln x - (D4)\mu}{\beta}\right) \quad (8)$$

where x = specified PGA value for individual chimney
μ = Natural Log value of fragility curve median
β = beta value in fragility curve analysis
Φ is the standard normal CDF operator

Table 3: Damage states and respective equations

Damage State	No Damage	Some Damage	Collapse
D – Level	D2	D2 – D4	D5
Equation	P3(B|A)	P4(B|A)	P5(B|A)

To account for the three different P(B|A) equations for the chimney damage states, the P(B|A) for a given GMM is equal to the product of three equations. This can be expressed as follows:

$$P(B|A) = P3(B|A) \cdot P4(B|A) \cdot P5(B|A) \quad (9)$$

This is completed for each ground motion model and provides a P(B|A) for that specific method taken evaluated.

Calculation of P(B) both methods

P(B) is calculated from the sum of all P(B|A) values produced by all ground motion models. This can be completed by only summing values from one fragility curve method and then comparing between methods or by integrating both methods through a full sum.

P(A) determination

The analysis considers two iterations of priors. The first iteration assumes each GMM prior distribution results in an equal likelihood. Therefore, using the Bayesian model to determine the likelihood of the respective GMM is based on only the observational data. The second iteration takes the prior distribution outlined in the logic tree weightings for GMMs in the NSHA18 outlined in Table 1.

V_{s30} consideration

The above process was repeated with four sets of PGA values calculated in OpenQuake for the various velocities: 270, 400, 560, 760 and 1100 m/s. Multiple velocities were considered and included in this study instead of a singular velocity due to not knowing the Vs30 at each site. This contributes to uncertainty within the analysis and one of the ways to consider this uncertainty was to repeat the analysis to examine relationships between velocity and GMM performance to determine if it can provide evidence for ground motion intensities.

Integration of Methods into a single P(A|B) value

To address epistemic uncertainty associated with which fragility curve is more 'correct', two methods of analysing P(A|B) values are used; averaging the values and integration into Bayesian analysis. The first assumption is that these two fragility models are equally probable. Therefore, the methodology outlined will simply be the average of P(A|B) for both fragility curve methods within their respective GMM. The alternative is to let the integration of fragility curve methods also provide insight into the most likely fragility curve paired with GMM. However, we decide not to proceed with this method due to the highly uncertain nature of fragility curves. We believe the Bayesian approach cannot tell us the most likely fragility curve. Velocity probabilities are also considered and calculated within the P(A|B). It was decided the Bayesian analysis can provide probabilistic insights into which velocity is more likely to be correct.

A Bayesian approach was undertaken separately for two different groups of GMMs. The first group analysed GMMs currently used in the NSHA18 to complete an independent assessment of only NSHA18 GMMs relative to each other. The second group consists of all the GMMs mentioned in this paper. This allowed discussion and analysis of all GMMs in the paper, while also allowing the analysis of only NSHA18 independent of the non-NSHA18 GMMs.

Results

Bayesian Inference of GMMs

A probability of collapse at the expected PGA value was computed for each chimney for all ten ground motion models using both fragility curve methods. All results of the Bayesian analysis can be seen in Table 4 and can be visualised in Figure 11. Columns 3 and 5 represent the NSHA18 Bayesian analysis, one without the expert elicitation priors and one without. Column 5 represents the Bayesian analysis that evaluated all GMMs outlined in this paper.

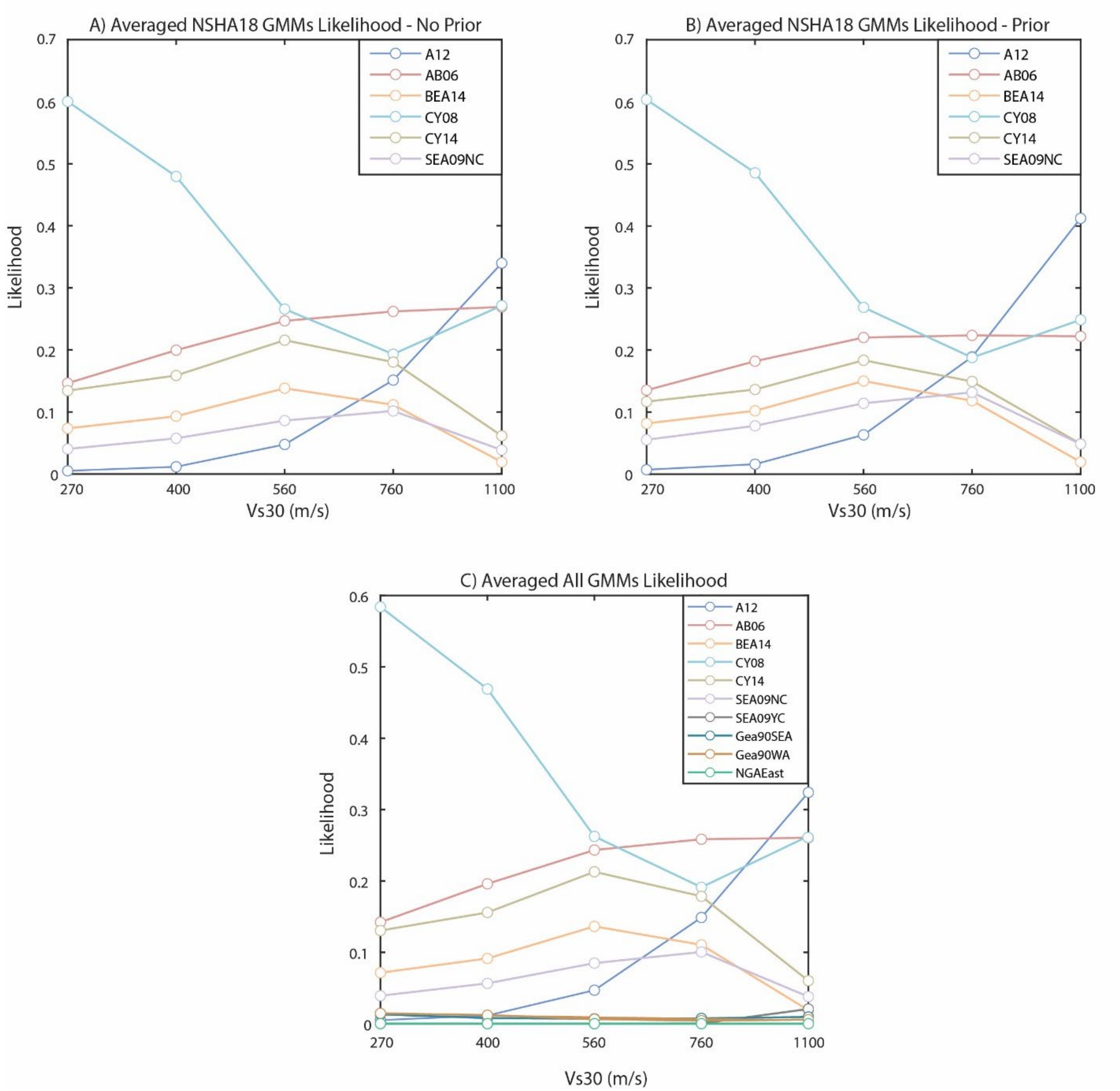

Figure 11: Results of Bayesian GMM likelihoods at all velocities assuming fragility curves are equally likely to be correct. Results display three Bayesian analyses, one incorporating the NSHA18 expert elicitations (priors: 11b) and one without (Uniform Prior / no prior: 11a and one considering all GMMs with no priors (11c)

Table 4: Bayesian Analysis results of NSHA18 GMMs and All GMMs assuming fragility curves are equally likely to be correct. Results display three Bayesian analyses, one incorporating the NSHA18 expert elicitations (priors), one without the NSHA18 priors and one with all GMMs.

Velocity (m/s) [weighting]	GMM	NSHA18 GMMS - Averaged Likelihood - Uniform Prior	NSHA18 GMMS - Averaged Likelihood - EE Prior	All GMMs - Averaged Likelihood
270 [0.129]	A12	0.005	0.007	0.005
	AB06	0.146	0.135	0.142
	BEA14	0.073	0.082	0.071
	CY08	0.6003	0.6036	0.584
	CY14	0.1343	0.1169	0.131
	SEA09NC	0.040	0.055	0.039
	Gea90SEA			0.013
	Gea90WA			0.014
	SEA09YC			0.000
	NGA-E			0.000
400 [0.218]	A12	0.012	0.016	0.011
	AB06	0.200	0.182	0.196
	BEA14	0.093	0.102	0.091
	CY08	0.480	0.486	0.469
	CY14	0.159	0.136	0.156
	SEA09NC	0.058	0.078	0.057
	Gea90SEA			0.008
	Gea90WA			0.012
	SEA09YC			0.000
	NGA-E			0.000
560 [0.249]	A12	0.048	0.063	0.047
	AB06	0.2468	0.220	0.243
	BEA14	0.138	0.150	0.136
	CY08	0.266	0.269	0.262
	CY14	0.216	0.184	0.213
	SEA09NC	0.086	0.114	0.085
	Gea90SEA			0.007
	Gea90WA			0.006
	SEA09YC			0.000
	NGA-E			0.000
760 [0.229]	A12	0.151	0.189	0.149
	AB06	0.262	0.224	0.258
	BEA14	0.112	0.118	0.110
	CY08	0.193	0.188	0.191
	CY14	0.180	0.149	0.179
	SEA09NC	0.102	0.132	0.101
	Gea90SEA			0.007
	Gea90WA			0.004
	SEA09YC			0.000
	NGA-E			0.000
1100 [0.1739]	A12	0.340	0.412	0.324
	AB06	0.269	0.222	0.260
	BEA14	0.019	0.020	0.019
	CY08	0.271	0.249	0.263
	CY14	0.061	0.049	0.060
	SEA09NC	0.039	0.048	0.038
	Gea90SEA			0.009
	Gea90WA			0.006
	SEA09YC			0.021
	NGA-E			0.000

Results and Discussion

At all V_{S30} values, there are two clusters of ground motion models that probabilistically match the observed chimney damage resultant from the Woods Point earthquake. GMMs selected for the NSHA18 for this tectonic region (A12, AB06, BEA14, CY08, CY14, and SEA09NC) outperform non-NSHA18 GMMs (NGA-E, GEA90SEA, GEA90WA, SEA09NC). NSHA18 GMM weightings are variable across Vs30 values. Variability could reflect the effect of epistemic uncertainties within the GMMs and/or fragility curves. Specifically, GMM computation in this study has an emphasis on median ground motion predictions, omitting the characterization of ground motion variability. Complex geology, GMMs not specifically curated for southeast Australia, source to site variations and incomplete catalogues all play an aspect in increasing uncertainty for each ground motion model. Variable likelihoods may also be a result of GMMs being statistically selected to represent this seismic context, therefore similar performance could be expected as per their use in the NSHA18. These models have been chosen to represent southeast Australia as they are meant to be applied to non-cratonic and SCR regions, and therefore, it is expected they would perform similarly. However, there are trends such as a statistical preference for A12 at high Vs30 vales, and CY08 vastly being the preference GMM at low Vs30s.

The most likely site class within the earthquake epicentral region is B to B/C (Figure 6) based on both the geology observed in the reconnaissance survey and the seismic site conditions map for Australia (McPherson, 2017; Wald and Allen, 2007; Heath et al., 2020). This suggests a Vs30 value ranging from 760 – 1100 m/s for the region of interest. At 760 m/s, the NSHA18 GMMs outperform the GMMs not currently included in the NSHA. At 1100 m/s, NSHA18 GMMs outperform non-NSHA18 GMMs with A12, AB06, and CY08 the most likely GMMs that matcfh the chimney damage observations. A12 is the statistically preferred model at 0.32. At low Vs30 values (270 & 400), the clear statistical preference is CY08 presumably because Vs30 scaling resulted in other GMMs overestimating the actual PGA within the epicentral region and therefore the Bayesian model would have expected more chimney damage to occur than was observed. CY08 is the second lowest PGA output on average, with the lowest being GEA90WA. We suggest that the outputs of CY08 at low velocities are similar to the PGAs within the epicentral region from the earthquake at a velocity range of 760 – 110 m/s.

The results of our analysis statistically preference three models: A12, AB06 and CY08. The A12 model is curated for southeastern Australia and uses a stochastic finite-fault simulation technique involving the use of reinterpreted source and attenuation parameters for small to moderate magnitude southeast Australian earthquakes. Similarly, the AB06 GMM uses a stochastic finite-fault simulation technique using earthquakes from the Eastern North American (ENA) region. Comparatively, A12 and AB06 models perform similarly due to similar simulation techniques and the ENA and SEA regions may be seismically analogous (Allen and Atkinson, 2007; Allen, 2012). A12 and AB06 produce similar SA, especially at low periods within 200 km from the epicentre and may be a factor in the similar performance of these models at the 1100 m/s velocity in the Bayesian model. Allen and Atkinson (2007) concluded that there is no significant difference in source characteristics of ENA and SEA earthquakes. This resulted in the inclusion of the AB06 within the NSHA18 and for use in SCRs. The CY08 model was adjusted for use within the 2015 Swiss Seismic Hazard map (Edwards et al., 2016). This variation of the model has been adopted within the NSHA18. Geological constituency of the deformed and thrusted Mesozoic sediment over crystalline basement (Pfiffner, 2021) with Silurian to early Middle Devonian sediment deformed and thrusted above basement in the Victorian Highlands (Fergusson et al., 1986) may yield similar seismic attenuation characteristics between the two regions.

The SEA09NC model is largely consistent and statistically places among the lower end of the NSHA18 models but outperforms non-NSHA18 models at all Vs30 values but 1100 m/s. Future consideration of NSHA logic tree weightings may consider the relative lowering of the SEA09NC model. The Yilgarn craton (SEA09YC) version of this GMM performs poorly and on average predicts the second highest expected PGA behind NGA-E, which should have resulted in more chimney failure. CY14 and BEA14 model represent the California region of the Western US. These models perform relatively well at the 560 – 760 m/s velocity range but, particularly BEA14, drastically decreases at the 1100 m/s range. This suggests attenuation within the Californian region may be higher than that of southeast Australia. Additionally, the CY14 model uses $Z_{1.0}$ and $Z_{2.5}$ inputs intended to model basin effects. This may be a contributing factor into the increased likelihood of this model within low velocity ranges (400 m/s). This decline may come at the expense of A12 in which becomes the highest performing model and trends higher as Vs30 increases. The Gaull et al., 1990 models (SEA and WA) both performed poorly. These models were not included in NSHA18 due to poor model performance against ground motion records and issues with the conversion of local magnitude to moment magnitude. This analysis provides further justification of the removal of these GMMs from the NSHA18. NGA-East is the worst performing model. We find that NGA-East likely overestimates ground motions within the epicentral region for the Woods Point earthquake. NGA-East also overestimated ground motions for Mw 5.2 2012 Moe, Australia earthquake sequence as inferred from comparison of instrumentally recorded ground motions against NGA-East predictions (Hoult et al., 2021b).

PGAs resulting from the Woods Point earthquake are best modelled by three GMMS, A12, AB06 and CY08 at a Vs30 of 1100 m/s. At 760 m/s, NSHA18 GMMs are more variable and represent similar variability as the weighting published in the NSHA. The weightings are not exact, but it should be considered that there is GMM variability over different Vs30 values and that this study only considers relatively near epicentral regions and doesn't cover the full GMM integration distance of 400 km. Additionally, this is a comparison of ground motion models against one earthquake and a full analysis should considered earthquakes of varying rupture type and magnitude. Additional data must be used to compliment the findings in this study to further inform earthquake hazard and thoroughly characterize GMM logic trees used in PSHAs.

Of the two-fragility curve models, the product of the probability of observed (*p(B|A)*) in Model 1 (Maison and McDonald, 2018) is greater than model 2 (see Appendix D). Model 2 is penalised for aiming to model chimney fragility damage at a higher resolution due to this fragility curve model having five damage states. Additionally, model one has a smaller sample size of chimneys resulting in the (*p(B|A)*) to be higher. Therefore, we favour the approach of averaging the *P(B|A)* values, through assigning equal probability of either fragility curve being correct, to evaluate the relative performance of GMMs. The purpose of this analysis is to evaluate GMMs and not fragility curves. There is insufficient information for a hierarchical analysis of both GMMs and fragility curves so the approach of equal weighting for the fragility curves is the most conservative choice. This paper presents a Bayesian approach to validating ground motion models using observed data in the form of chimney fragility curves. It suggests for a range of site class velocities, a preferred logic tree weighting for the various GMMs at distances of 13 to 60 km for the Woods Point earthquake. As part of the NSHA18, GMMs can be integrated at distances of up to 400 km.

However, when considering the likelihood of each GMM without the prior distribution, it suggests confidence and solidifies the use of the current logic tree weightings for PSHAs. Consideration could be given to refining the weightings of GMMs in future national seismic hazard models for Australia based on our analysis, although we note that this analysis only uses the Woods Point earthquake.

Conclusion

In regions of limited seismometer coverage such as SCRs, a Bayesian approach in assessing chimney fragility in response to an earthquake may be used to evaluate the relative performance of commonly used GMMs in PSHAs. The utilized Bayesian approach of independently derived probabilistic chimney fragility values supports the current NSHA18 PSHA relative weightings but highlights the consideration for ongoing refinement of weightings in a future NSHA. PGAs within the Woods Point earthquake epicentral region are best modelled by the predicted median outputs from three GMMs: A12, AB06 and CY14. NSHA18 GMMs outperformed other GMMs for the Woods Point earthquake based on the ground motion proxies used here.

References

Allen, T., 2012. Stochastic Ground-motion Prediction Equations for southeastern Australian Earthquakes using Updated Source and Attenuation Parameters, Geoscience Australia, Canberra, Record 2012/69.

Allen, T. I., & Atkinson, G. M., 2007. Comparison of earthquake source spectra and attenuation in eastern North America and southeastern Australia. Bulletin of the Seismological Society of America, 97(4), 1350-1354.

Allen, T., A. Carapetis, J. Bathgate, H. Ghasemi, T. Pejić, and A. Moseley, 2019b. Real-time community internet intensity maps and ShakeMaps for Australian earthquakes, Australian Earthquake Engineering Society 2019 Conference, Newcastle, New South Wales.

Allen, T., A. Carapetis, J. Bathgate, H. Ghasemi, T. Pejić, and A. Moseley, 2019. Real-time community internet intensity maps and ShakeMaps for Australian earthquakes, Australian Earthquake Engineering Society 2019 Conference, Newcastle, New South Wales. https://aees.org.au/wp-content/uploads/2019/12/29-Trevor-Allen.pdf

Allen, T., Griffin, J., Clark, D. 2018. The 2018 National Seismic Hazard Assessment for Australia: Model input files. Record 2018/032. Geoscience Australia, Canberra. http://dx.doi.org/10.11636/Record.2018.032

Allen, T., Griffin, J., Leonard, M., Clark, D., Ghasemi, H. 2018. The 2018 National Seismic Hazard Assessment: Model overview. Record 2018/027. Geoscience Australia, Canberra. http://dx.doi.org/10.11636/Record.2018.027

Allen, T., H. Ghasemi, and J. Griffin, 2021. Exploring Australian hazard map exceedance using an atlas of historical ShakeMaps, Australian Earthquake Engineering Society 2021 Virtual Conference. https://aees.org.au/wp-content/uploads/2022/02/13-Trevor-Allen.pdf

Allen, T., Leonard, M., & Collins, C., 2012. The 2012 Australian Seismic Hazard Map–Catalogue and Ground Motion Prediction Equations. In Proceedings of the 2011 Australian Earthquake Engineering Society Conference, Barossa Valley, SA (this volume).

Atkinson, G. M., & Boore, D. M., 2006. Earthquake ground-motion prediction equations for eastern North America. Bulletin of the seismological society of America, 96(6), 2181-2205.

Bayes, T. 1764. "An Essay Toward Solving a Problem in the Doctrine of Chances", Philosophical Transactions of the Royal Society of London 53, 370-418.

Bommer, J. J., Douglas, J., Scherbaum, F., Cotton, F., Bungum, H., & Fäh, D.,2010. On the selection of ground-motion prediction equations for seismic hazard analysis. Seismological Research Letters, 81(5), 783-793.

Boore, D. M., Stewart, J. P., Seyhan, E., & Atkinson, G. M., 2014. NGA-West2 equations for predicting PGA, PGV, and 5% damped PSA for shallow crustal earthquakes. Earthquake Spectra, 30(3), 1057-1085.

Chiou, B. S. J., & Youngs, R. R., 2014. Update of the Chiou and Youngs NGA model for the average horizontal component of peak ground motion and response spectra. Earthquake Spectra, 30(3), 1117-1153.

Federal Emergency Management Agency (FEMA), 2018. Seismic Performance Assessment of Buildings Volume 1– Implementation Guide, Tech. Rep, FEMA P-58-1, Washington, D.C.

Fergusson, C. L., Gray, D. R., & Cas, R. A., 1986. Overthrust terranes in the Lachlan fold belt, southeastern Australia. Geology, 14(6), 519-522.

Gaull, B. A., Michael-Leiba, M. O., & Rynn, J. M. W., 1990. Probabilistic earthquake risk maps of Australia. Australian Journal of Earth Sciences, 37(2), 169-187.

Ghasemi, H. and Allen, T. 2018. Selection and ranking of ground-motion models for the 2018 National Seismic Hazard Assessment of Australia: Summary of ground-motion data, methodology and outcomes. Record 2018/029. Geoscience Australia, Canberra. http://dx.doi.org/10.11636/Record.2018.029

Goulet, C. A., Bozorgnia, Y., Kuehn, N., Al Atik, L., Youngs, R. R., Graves, R. W., & Atkinson, G. M., 2021. NGA-East ground-motion characterization model Part I: Summary of products and model development. Earthquake Spectra, 37(1_suppl), 1231-1282.

Griffin, J. D., T. I. Allen, and M. C. Gerstenberger., 2020. Seismic hazard assessment in Australia: can structured expert elicitation achieve consensus in the "land of the fair go"?, Seismol. Res. Lett. 91, 859–873, doi: 10.1785/0220190186.

Griffin, J., Gerstenberger, M., Allen, T., Clark, D., Cuthbertson, R., Dimos, A., Gibson, G., Ghasemi, H., Hoult, R., Lam, N., Leonard, M., Mote, T., Quigley, M., Somerville, P., Sinadinovski, C., Stirling, M., Venkatesan, S., 2018. Expert elicitation of model parameters for the 2018 National Seismic Hazard Assessment - Summary of workshop, methodology and outcomes. Record 2018/028. Geoscience Australia, Canberra. http://dx.doi.org/10.11636/Record.2018.028

Heath, D. C., D. J. Wald, C. B. Worden, E. M. Thompson, and G. M. Smoczyk., 2020. A global hybrid VS30 map with a topographic slope–based default and regional map insets, Earthquake Spectra 36, 1570-1584, doi: 10.1177/8755293020911137.

Henshaw, P., Burton, C., Butler, L., Crowley, H., Danciu, L., Nastasi, M., ... & Wyss, B., 2013. Openquake, a platform for collaborative seismic hazard and risk assessment. In EGU General Assembly Conference Abstracts (pp. EGU2013-10547).

Hoult, R. D., Pascale, A., Jones, A., & Allen, T, 2021a. The MW 5.9 Woods Point Earthquake: A Preliminary Investigation of the Ground Motion Observations.

Hoult, R., Allen, T., Borleis, E., Peck, W., & Amirsardari, A., 2021b. Source and attenuation properties of the 2012 Moe, southeastern Australia, earthquake sequence. Seismological Research Letters, 92(2A), 1112-1128.

Joyce, J. 2003. Bayes' theorem. E.N. Zalta (Ed.), Stanford Encyclopedia of Philosophy, Stanford University, Stanford (2003)

Kaklamanos, J., L. G. Baise, and D. M. Boore., 2011. Estimating unknown input parameters

Krawinkler, H., Osteraas, J. D., McDonald, B. M., & Hunt, J. P.., 2012. Development of damage fragility functions for URM chimneys and parapets. In 15th World Conference in Earthquake Engineering, Lisbon, Portugal.

La Greca, J. and Quigley, M., 2021 Survey of environmental and infrastructure damage from the September 2021 Mw 5.9 Woods Point earthquake, Victoria, Australia: Part 2. In: Earthquake Engineering Research Institute – Australian Earthquake Engineering Society – New Zealand Society of Earthquake Engineering Joint Learning from Earthquakes Clearinghouse: Woods Point, Australia Earthquake. 64 pg.

Lallemant, D., Kiremidjian, A., & Burton, H., 2015. Statistical procedures for developing earthquake damage fragility curves. Earthquake Engineering & Structural Dynamics, 44(9), 1373-1389.

Leonard, M., Burbidge, D. R., Allen, T. I., Robinson, D. J., McPherson, A., Clark, D., & Collins, C. D. N., 2014. The challenges of probabilistic seismic-hazard assessment in stable continental interiors: An Australian example. Bulletin of the Seismological Society of America, 104(6), 3008-3028.

Maison, B., & McDonald, B., 2018. Fragility curves for residential masonry chimneys. Earthquake Spectra, 34(3), 1001-1023. DOI: 10.1193/021217EQS028EP

McCue, K. Historical earthquakes in Victoria: A Revised List. Australian Earthquake Engineering Society

McPherson, A.A. 2017. A revised seismic site conditions map for Australia. Record 2017/012. Geoscience Australia, Canberra. http://dx.doi.org/10.11636/Record.2017.012

Moon, L., Dizhur, D., Senaldi, I., Derakhshan, H., Griffith, M., Magenes, G., & Ingham, J., 2014. The demise of the URM building stock in Christchurch during the 2010–2011 Canterbury earthquake sequence. Earthquake Spectra, 30(1), 253-276.

Pagani, M., Monelli, D., Weatherill, G., Danciu, L., Crowley, H., Silva, V., Henshaw, P., Butler, R., Nastasi, M., Panzeri, L., Simionato, M., and Vigano, D., 2014. OpenQuake Engine: an open hazard (and risk) software for the Global Earthquake Model, Seismol. Res. Lett. 85, 692–702, doi: 10.1785/0220130087.

Pfiffner, O. A., 2021. The Geology of Switzerland. In Landscapes and Landforms of Switzerland (pp. 7-30). Springer, Cham.

Quigley, M., Pascale, A., Clark, D., Allen, T., 2021. Wednesday 22 September 2021 Mw 5.9 Woods Point earthquake – Information Sheet. Access at: http://learningfromearthquakes.org/2021-09-22-australia/images/2021_09_22-australia/pdfs/REPORT_EQ_27_SEPT_2021_short.TA.pdf

Somerville, P., R. Graves, N. Collins, S.-G. Song, S. Ni, and P. Cummins., 2009. Source and ground motion models for Australian earthquakes, Australian Earthquake Engineering Society 2009 Conference, Newcastle, New South Wales

van de Schoot, R., Depaoli, S., King, R., Kramer, B., Märtens, K., Tadesse, M. G., ... & Yau, C., 2021. Bayesian statistics and modelling. Nature Reviews Methods Primers, 1(1), 1-26.

Wald, D. J., and T. I. Allen., 2007. Topographic slope as a proxy for seismic site conditions and amplification, Bull. Seismol. Soc. Am. 97, 1379-1395, DOI: 10.1785/0120060267.

Wald, D.J., Jaiswal, K.S., Marano, K.D., Bausch, D.B., and Hearne, M.G., 2010, PAGER—Rapid assessment of an earthquake's impact: U.S. Geological Survey Fact Sheet 2010–3036, 4 p. Revised November, 2011.

Appendix A: Surveyed chimneys

Chimney Number	1	Image
X	146.1492917	
Y	-37.35309722	
Z	318.216	
Relative Mortar Condition	Medium	
Damage State	No Damage	
D – Level	2	

Maison and McDonald (2018) Fragility Curve	This Paper Fragility Curve
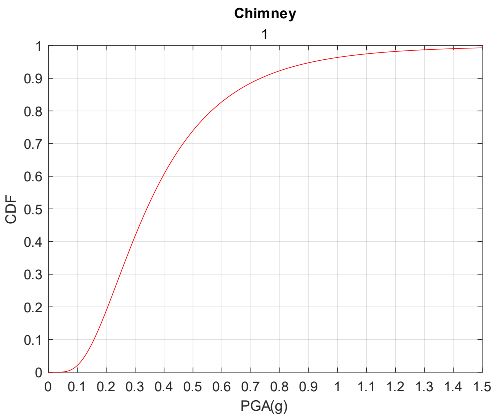	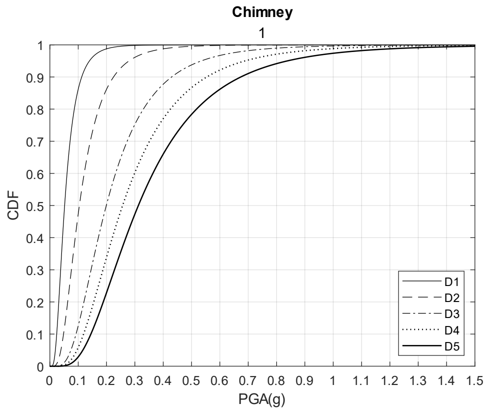

Chimney Number	2	Image
X	146.1377417	
Y	-37.30203611	
Z	305.557	
Relative Mortar Condition	Medium	
Damage State	No Damage	
D – Level	2	

Maison and McDonald (2018) Fragility Curve	This Paper Fragility Curve
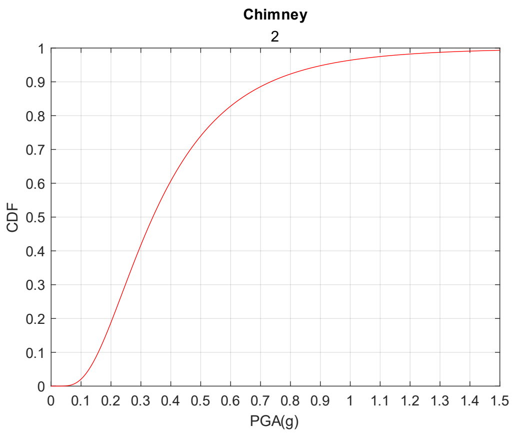	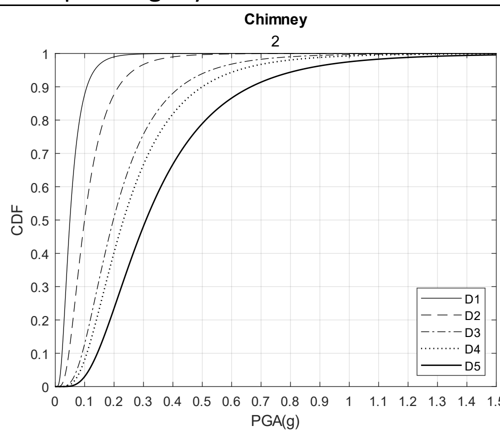

Chimney Number	3
X	146.1377417
Y	-37.30203611
Z	305.557
Relative Mortar Condition	Medium
Damage State	No Damage
D – Level	2

Image

Maison and McDonald (2018) Fragility Curve

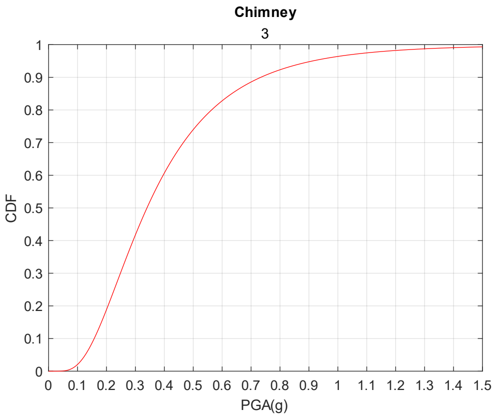

This Paper Fragility Curve

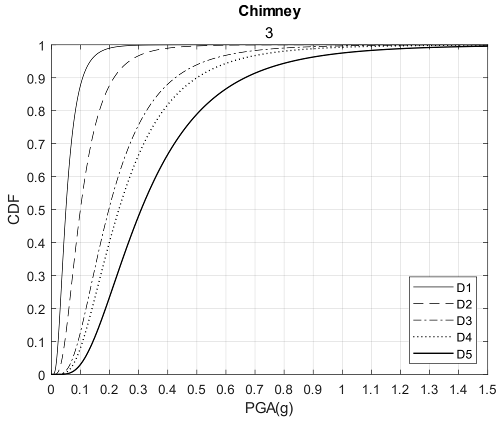

Chimney Number	4
X	146.1424556
Y	-37.30173889
Z	306.388
Relative Mortar Condition	Weak
Damage State	No Damage
D – Level	2

Image

Maison and McDonald (2018) Fragility Curve

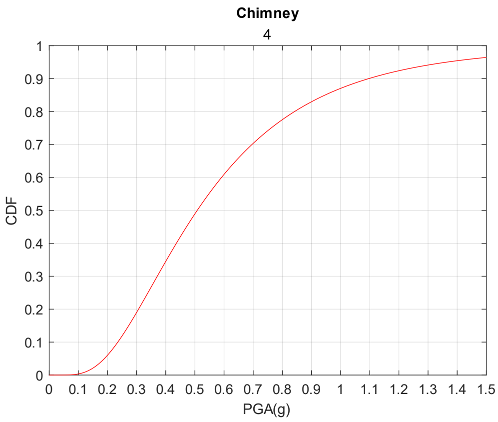

This Paper Fragility Curve

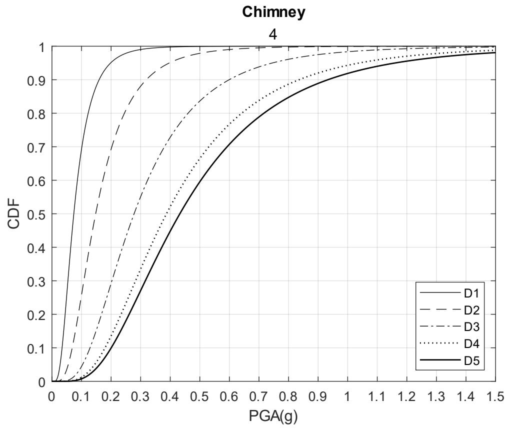

Chimney Number	5	Image
X	146.1431	
Y	-37.3023	
Z	302.989	
Relative Mortar Condition	Weak	
Damage State	Minimal Cracking	
D – Level	2 - 4	

Maison and McDonald (2018) Fragility Curve

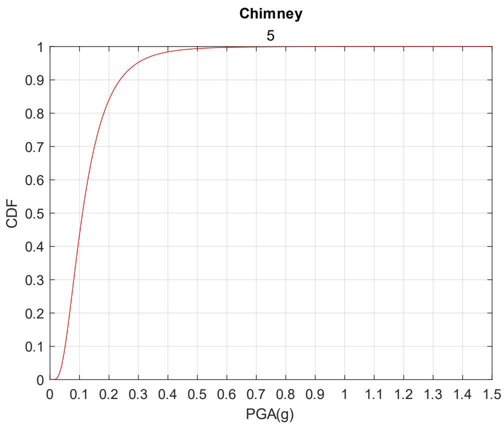

This Paper Fragility Curve

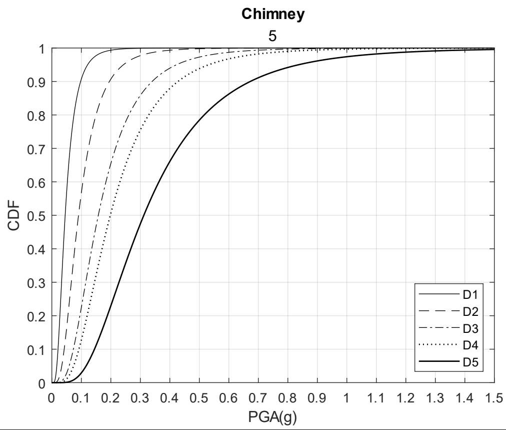

Chimney Number	6	Image
X	146.1431	
Y	-37.3023	
Z	302.989	
Relative Mortar Condition	Weak	
Damage State	No Damage	
D – Level	2	

Maison and McDonald (2018) Fragility Curve

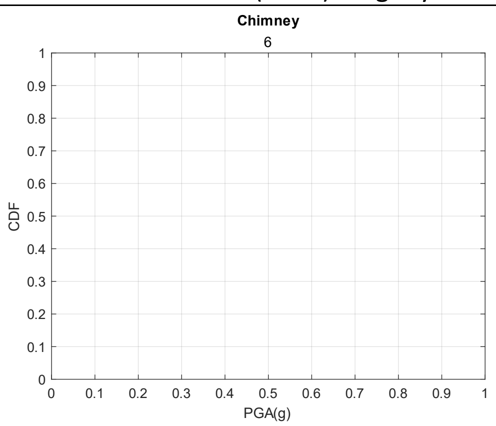

This Paper Fragility Curve

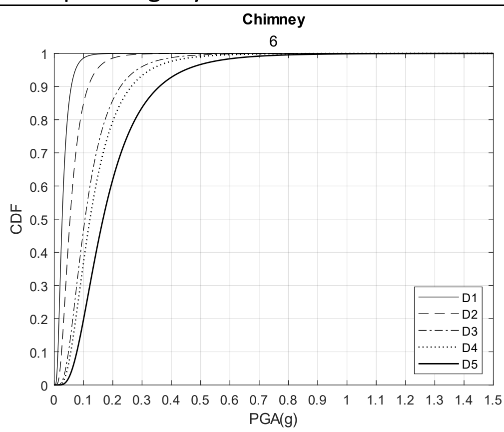

Chimney Number	7
X	146.1389
Y	-37.3024
Z	302.646
Relative Mortar Condition	Medium
Damage State	No Damage
D – Level	2

Image

Maison and McDonald (2018) Fragility Curve

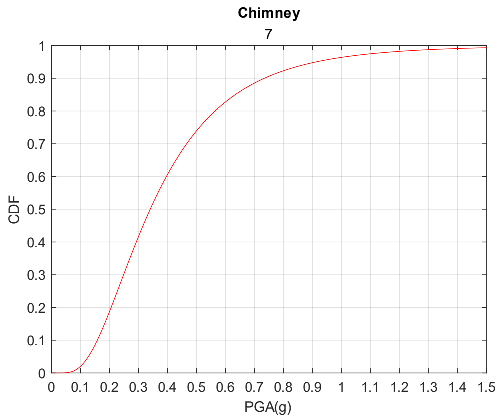

This Paper Fragility Curve

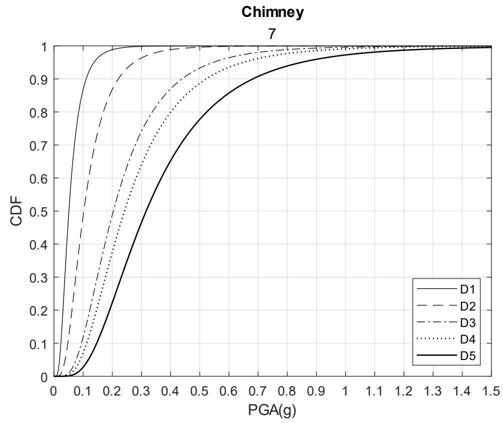

Chimney Number	8
X	146.1554
Y	-37.3577
Z	327.737
Relative Mortar Condition	Weak
Damage State	Minimal Cracking
D – Level	2 - 4

Image

Maison and McDonald (2018) Fragility Curve

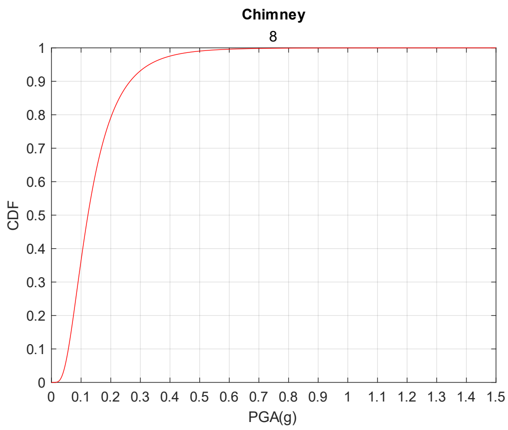

This Paper Fragility Curve

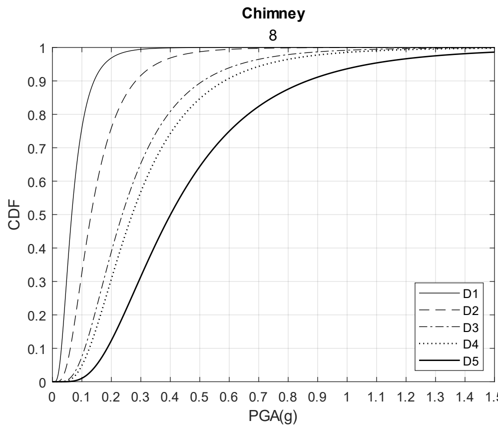

Chimney Number	9	Image
X	146.1554	
Y	-37.3577	
Z	327.737	
Relative Mortar Condition	Weak	
Damage State	Minimal Cracking	
D – Level	2 – 4	

Maison and McDonald (2018) Fragility Curve

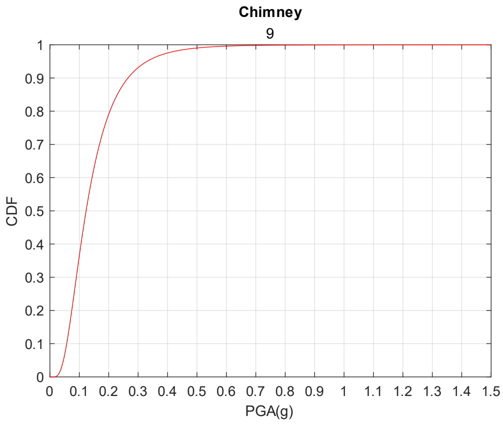

This Paper Fragility Curve

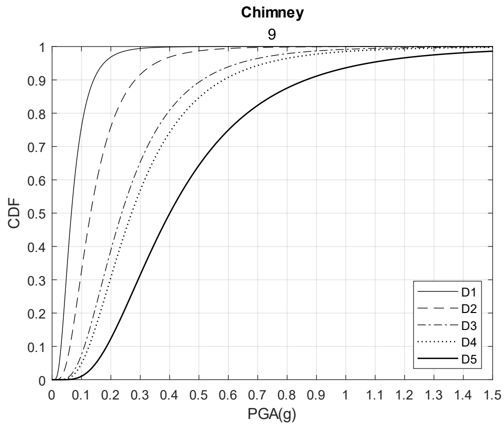

Chimney Number	10	Image
X	146.1876	
Y	-37.4705	
Z	507.4	
Relative Mortar Condition	Extremely Poor	
Damage State	No Damage	
D – Level	2	

Maison and McDonald (2018) Fragility Curve

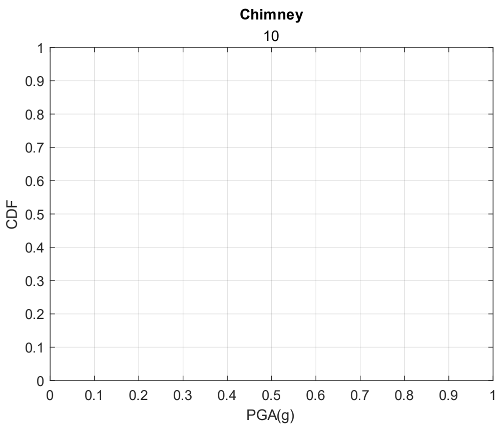

This Paper Fragility Curve

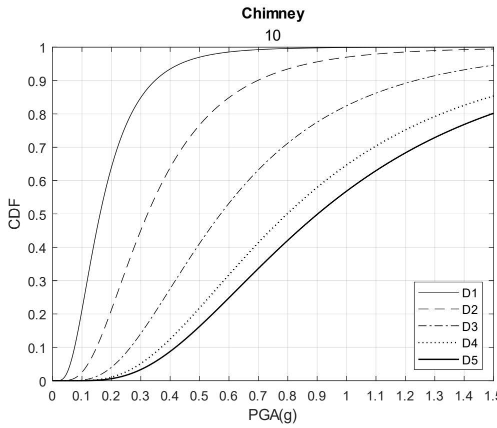

Chimney Number	11	Image
X	146.1994	
Y	-37.4974	
Z	665.797	
Relative Mortar Condition	Extremely Poor	
Damage State	No Damage	
D – Level	2	

Maison and McDonald (2018) Fragility Curve

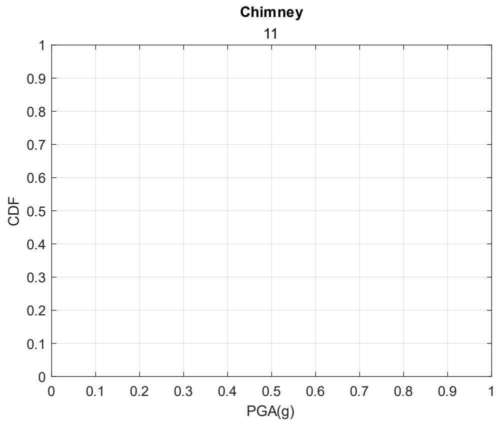

This Paper Fragility Curve

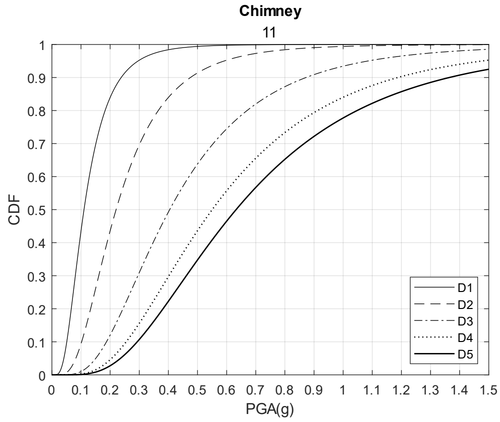

Chimney Number	12	Image
X	146.2494	
Y	-37.5654	
Z	679.494	
Relative Mortar Condition	Weak	
Damage State	Minimal cracking	
D – Level	2 – 4	

Maison and McDonald (2018) Fragility Curve

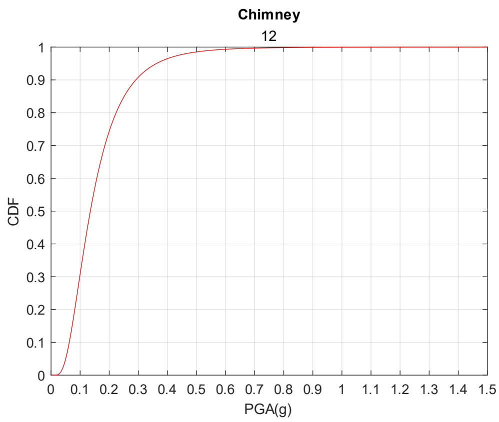

This Paper Fragility Curve

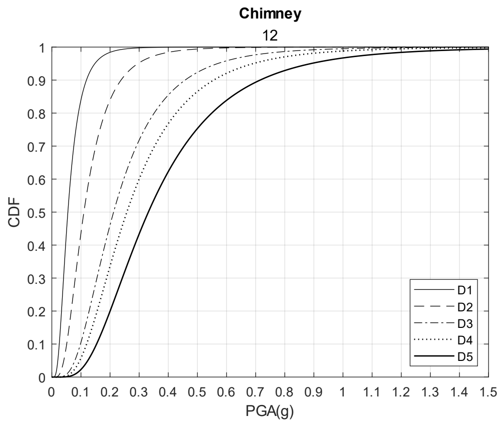

Chimney Number	13	Image
X	146.2496	
Y	-37.5657	
Z	683.103	
Relative Mortar Condition	Medium	
Damage State	No Damage	
D – Level	2	
Maison and McDonald (2018) Fragility Curve		This Paper Fragility Curve
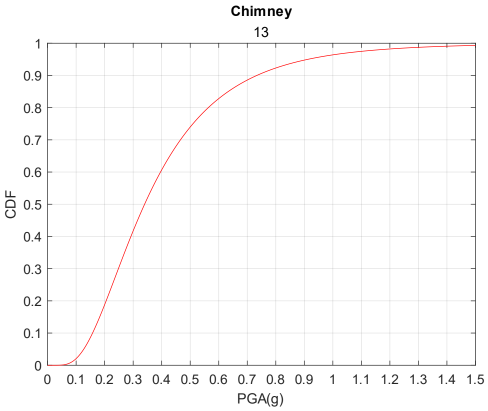		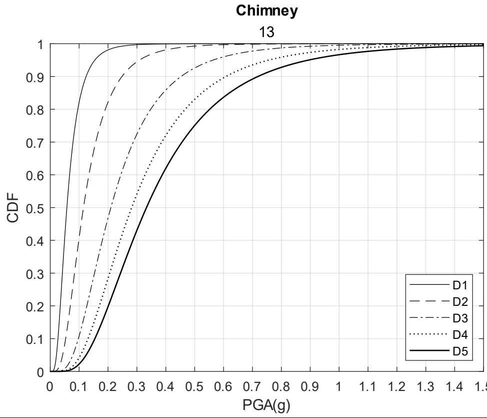

Chimney Number	14	Image
X	146.2496	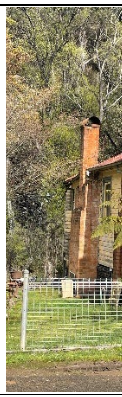
Y	-37.5657	
Z	683.103	
Relative Mortar Condition	Medium	
Damage State	No Damage	
D – Level	2	
Maison and McDonald (2018) Fragility Curve		This Paper Fragility Curve
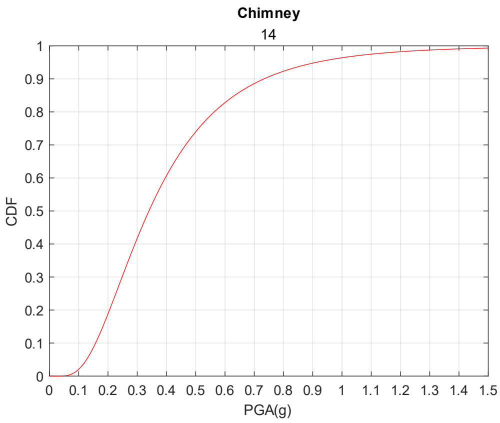		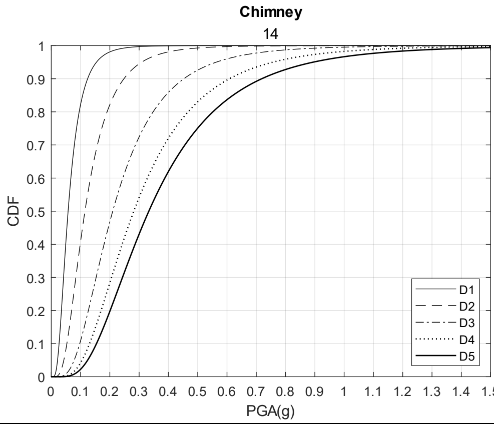

Chimney Number	15
X	146.2509
Y	-37.5674
Z	686.879
Relative Mortar Condition	Medium
Damage State	No Damage
D – Level	2

Image

Maison and McDonald (2018) Fragility Curve

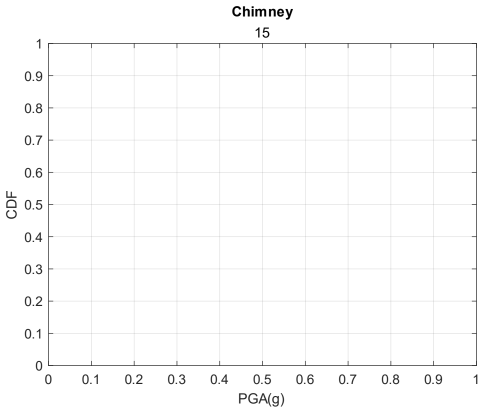

This Paper Fragility Curve

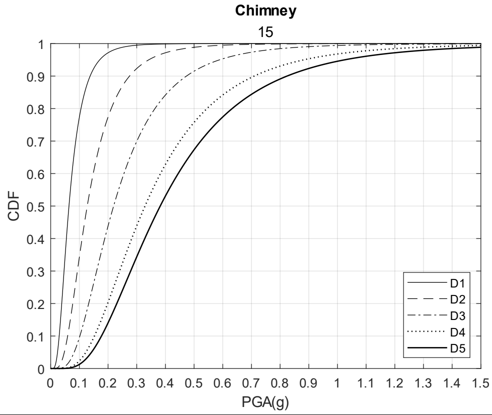

Chimney Number	16
X	146.2546
Y	-37.5715
Z	719.573
Relative Mortar Condition	Weak
Damage State	No Damage
D – Level	2

Image

Maison and McDonald (2018) Fragility Curve

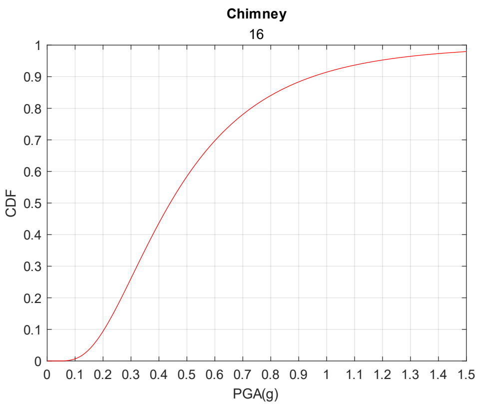

This Paper Fragility Curve

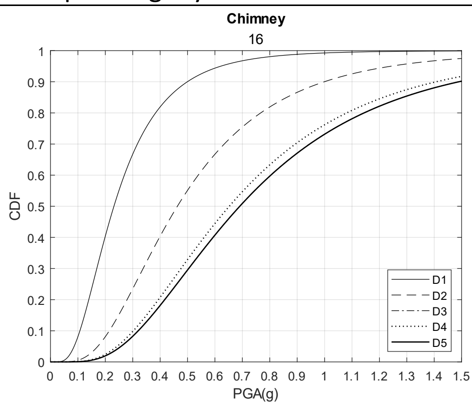

Chimney Number	17
X	146.2539
Y	-37.5708
Z	702.123
Relative Mortar Condition	Weak
Damage State	Collapsed
D – Level	5

Image

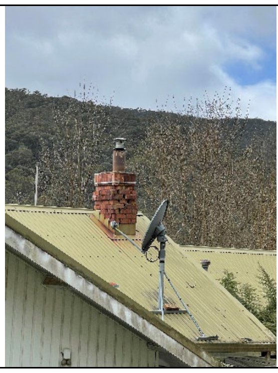

Maison and McDonald (2018) Fragility Curve

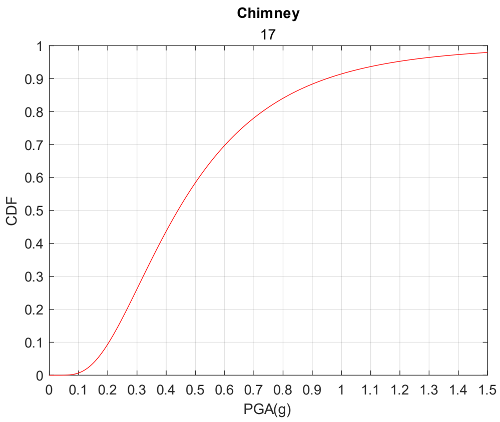

This Paper Fragility Curve

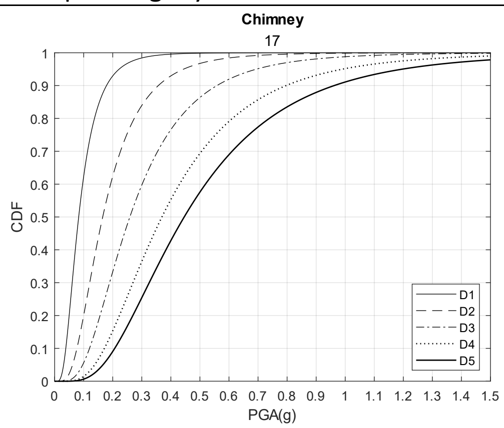

Chimney Number	18
X	146.2538
Y	-37.5708
Z	703.569
Relative Mortar Condition	Medium
Damage State	No Damage
D – Level	2

Image

Maison and McDonald (2018) Fragility Curve

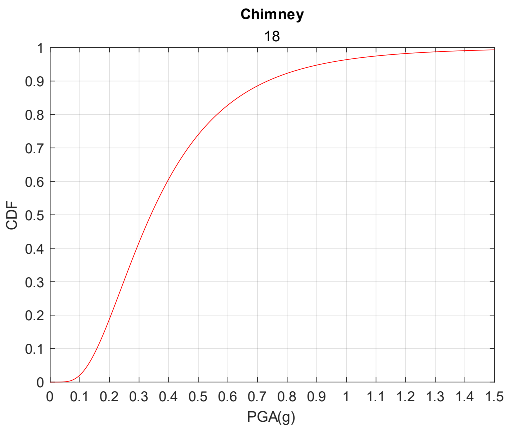

This Paper Fragility Curve

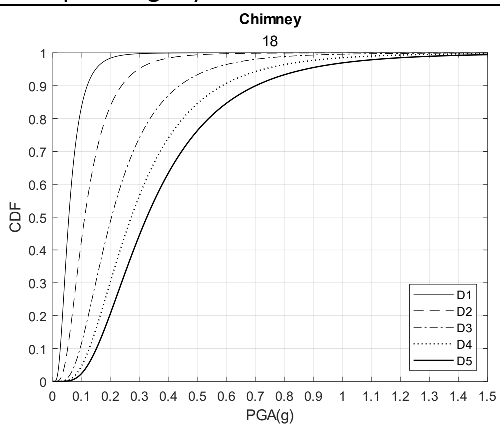

Chimney Number	19
X	146.2538
Y	-37.5708
Z	703.569
Relative Mortar Condition	Medium
Damage State	No Damage
D – Level	2

Image

Maison and McDonald (2018) Fragility Curve

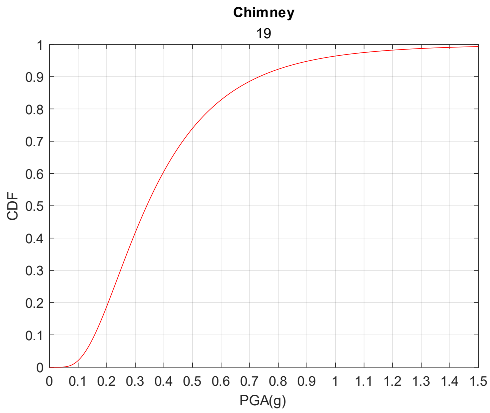

This Paper Fragility Curve

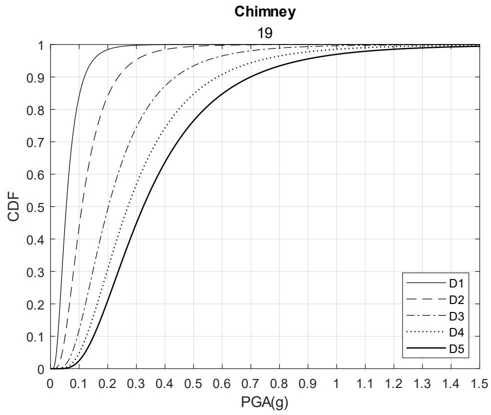

Chimney Number	20
X	146.2538
Y	-37.5708
Z	703.569
Relative Mortar Condition	Medium
Damage State	No Damage
D – Level	2

Image

Maison and McDonald (2018) Fragility Curve

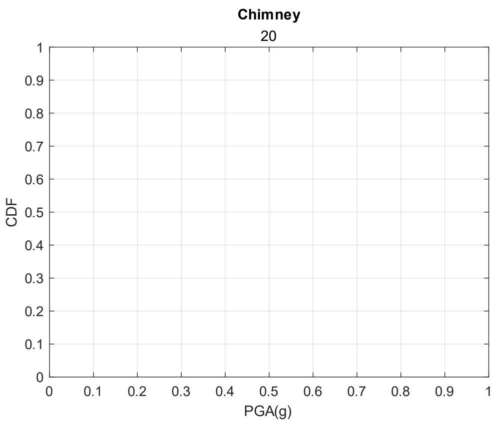

This Paper Fragility Curve

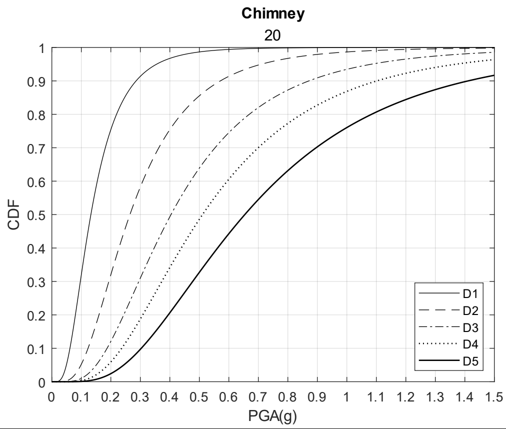

Chimney Number	21	Image
X	146.1875	
Y	-37.4726	
Z	518.788	
Relative Mortar Condition	Extremely Poor	
Damage State	Severe	
D – Level	5	

Maison and McDonald (2018) Fragility Curve	This Paper Fragility Curve

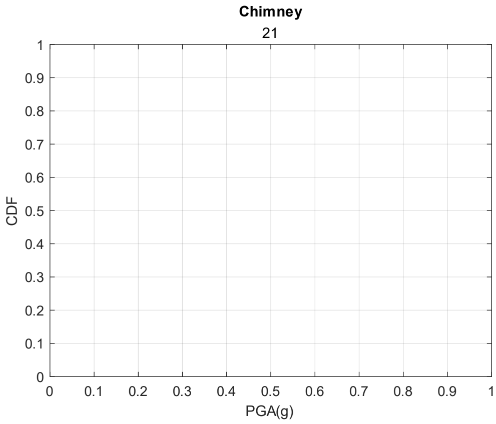

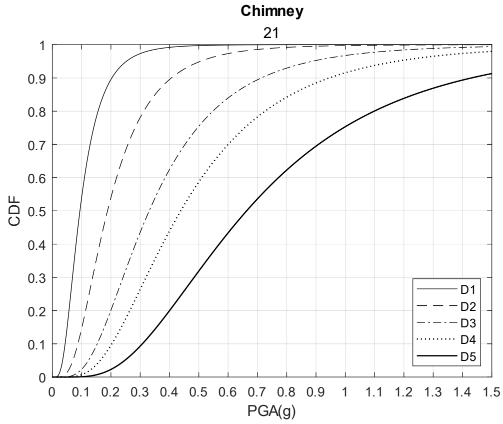

Chimney Number	22	Image
X	146.1877	
Y	-37.4706	
Z	510.143	
Relative Mortar Condition	Extremely Poor	
Damage State	No Damage	
D – Level	2	

Maison and McDonald (2018) Fragility Curve	This Paper Fragility Curve

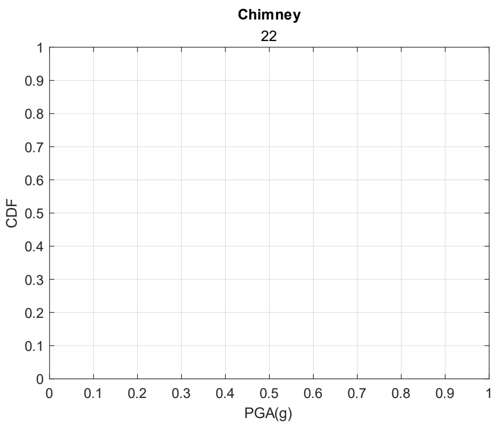

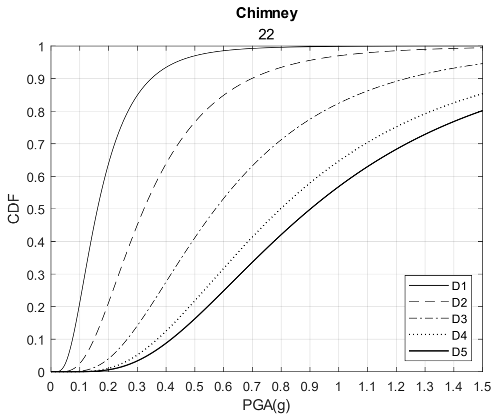

Chimney Number	23	Image
X	146.1402	
Y	-37.3026	
Z	294.077	
Relative Mortar Condition	Weak	
Damage State	No Damage	
D – Level	2	

Maison and McDonald (2018) Fragility Curve

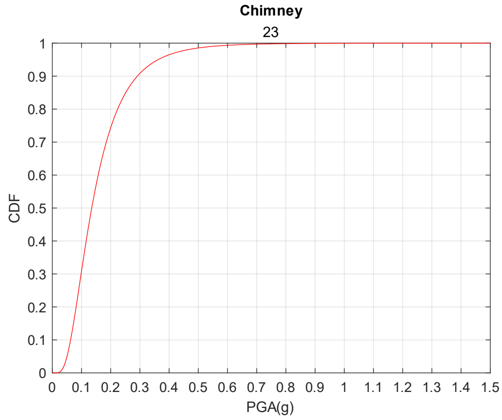

This Paper Fragility Curve

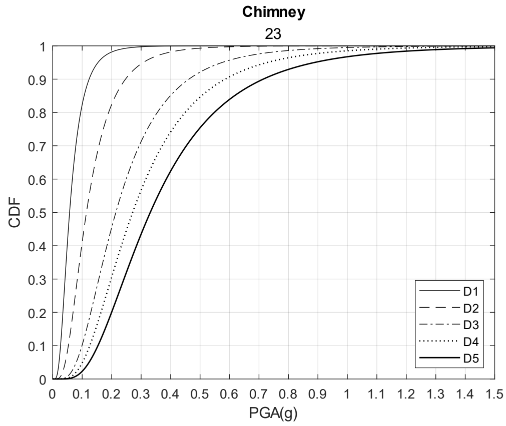

Chimney Number	24	Image
X	146.1348	
Y	-37.309	
Z	304.897	
Relative Mortar Condition	Weak	
Damage State	No Damage	
D – Level	2	

Maison and McDonald (2018) Fragility Curve

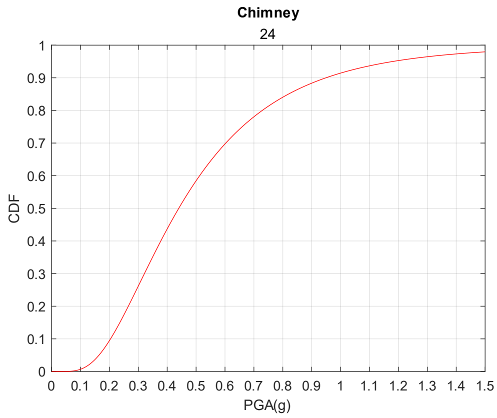

This Paper Fragility Curve

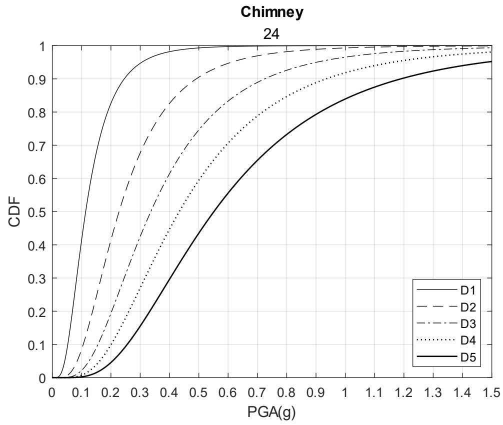

Chimney Number	25	Image
X	146.254	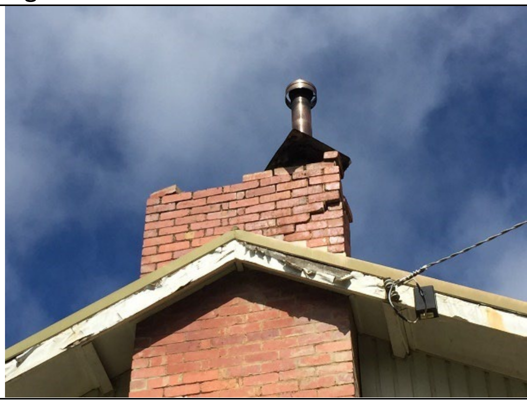
Y	-37.5707	
Z	707	
Relative Mortar Condition	Weak	
Damage State	Cracking	
D – Level	2 - 4	

Maison and McDonald (2018) Fragility Curve	This Paper Fragility Curve

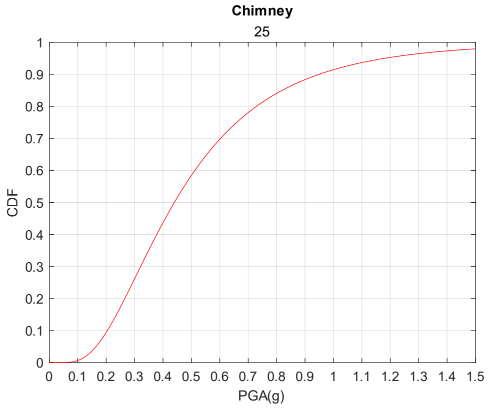

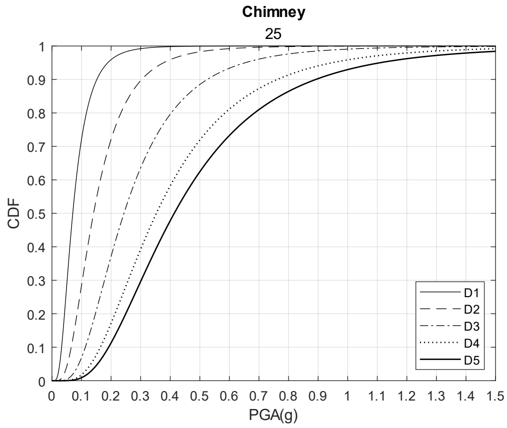

Chimney Number	26	Image
X	146.2544	
Y	-37.5708	
Z	706	
Relative Mortar Condition	Weak	
Damage State	Collapse	
D – Level	5	

Maison and McDonald (2018) Fragility Curve	This Paper Fragility Curve

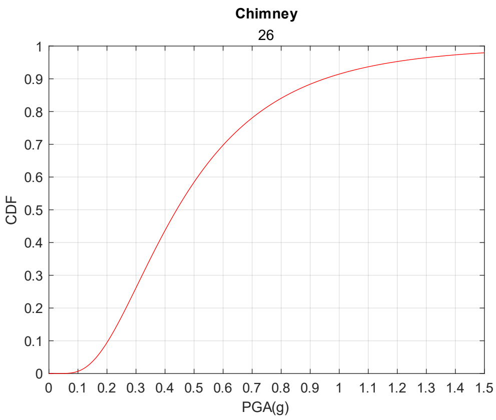

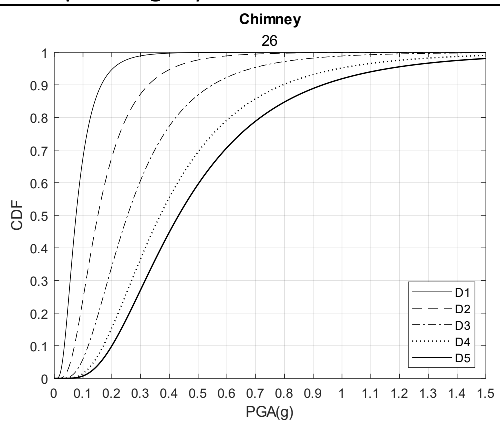

Chimney Number	27
X	146.149
Y	-37.3525
Z	349
Relative Mortar Condition	Medium
Damage State	No Damage
D – Level	2

Image

Maison and McDonald (2018) Fragility Curve

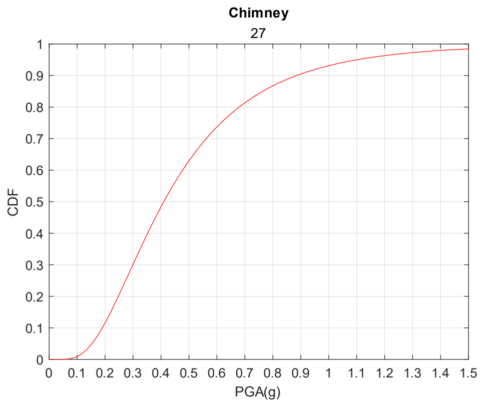

This Paper Fragility Curve

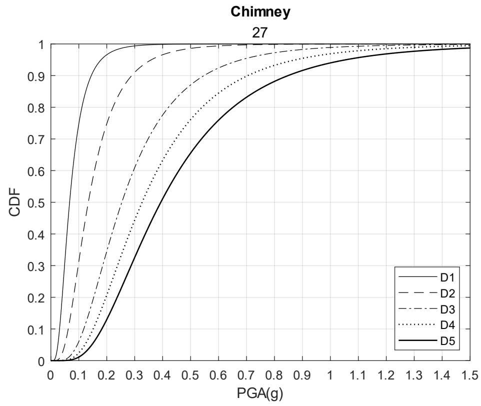

Chimney Number	28
X	146.1371
Y	-37.3037
Z	
Relative Mortar Condition	Weak
Damage State	No Damage
D – Level	2

Image

Maison and McDonald (2018) Fragility Curve

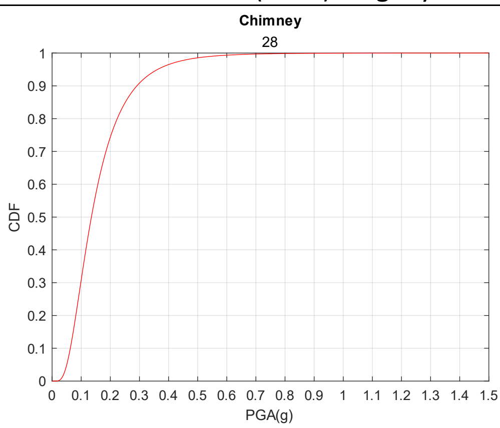

This Paper Fragility Curve

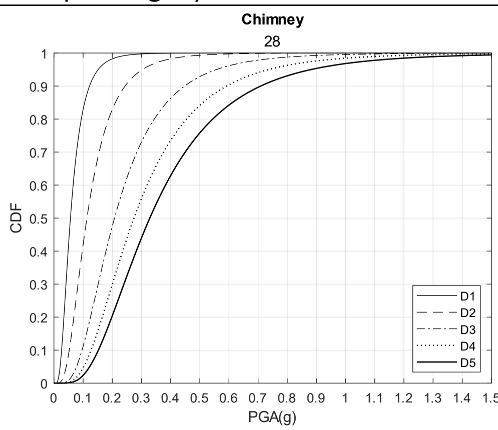

Chimney Number	29	Image
X	146.1371	
Y	-37.3037	
Z		
Relative Mortar Condition	Weak	
Damage State	No Damage	
D – Level	2	
Maison and McDonald (2018) Fragility Curve		This Paper Fragility Curve
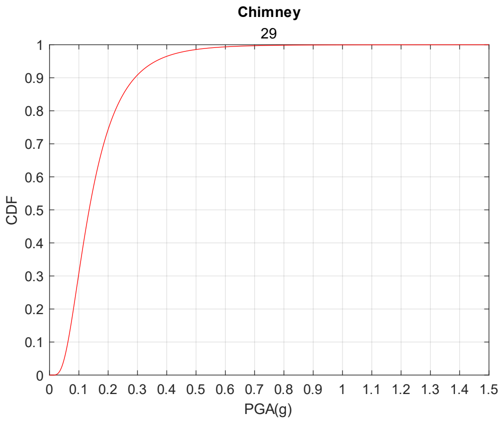		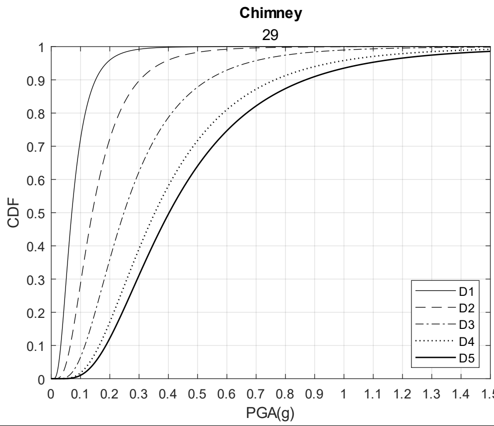

Chimney Number	30	Image
X	145.7119	
Y	-36.9763	
Z	337.357	
Relative Mortar Condition	Medium	
Damage State	No Damage	
D – Level	2	
Maison and McDonald (2018) Fragility Curve		This Paper Fragility Curve
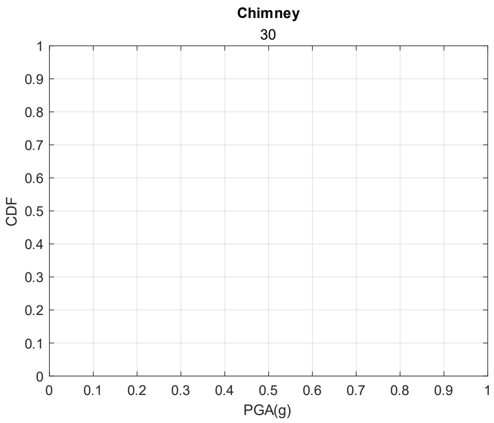		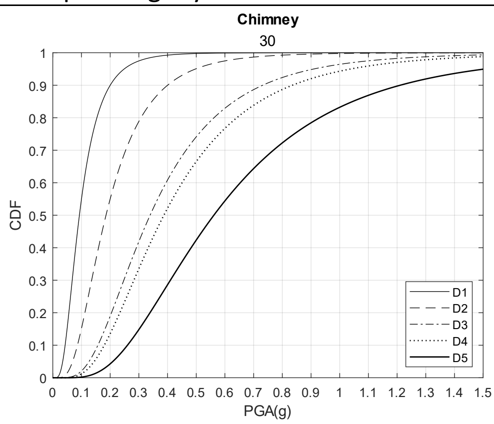

Chimney Number	31	Image
X	145.7119	
Y	-36.9763	
Z	337.357	
Relative Mortar Condition	Weak	
Damage State	No Damage	
D – Level	2	

Maison and McDonald (2018) Fragility Curve

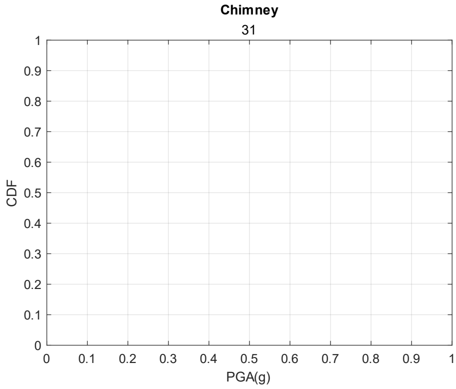

This Paper Fragility Curve

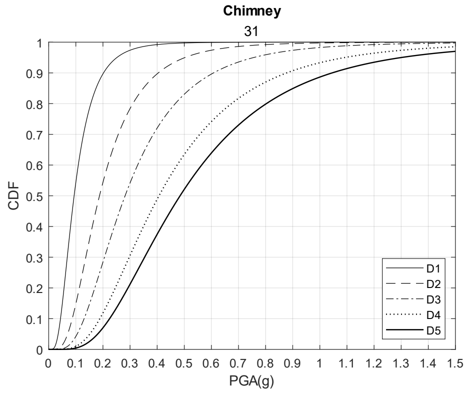

Chimney Number	32	Image
X	146.1395	
Y	-37.301	
Z	313.9	
Relative Mortar Condition	Good	
Damage State	No Damage	
D – Level	2	

Maison and McDonald (2018) Fragility Curve

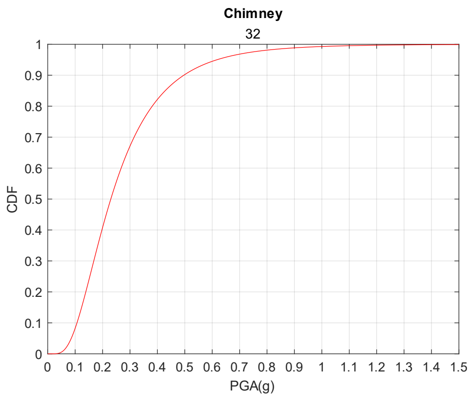

This Paper Fragility Curve

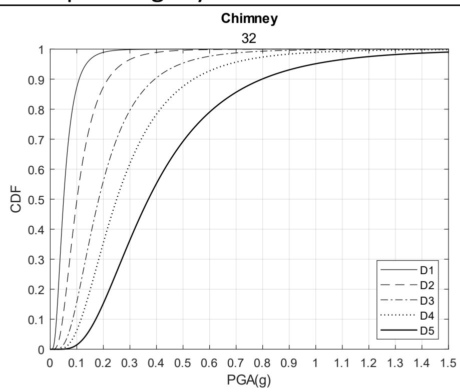

Chimney Number	33
X	146.1394
Y	-37.3005
Z	315.99
Relative Mortar Condition	Good
Damage State	No Damage
D – Level	2

Image

Maison and McDonald (2018) Fragility Curve

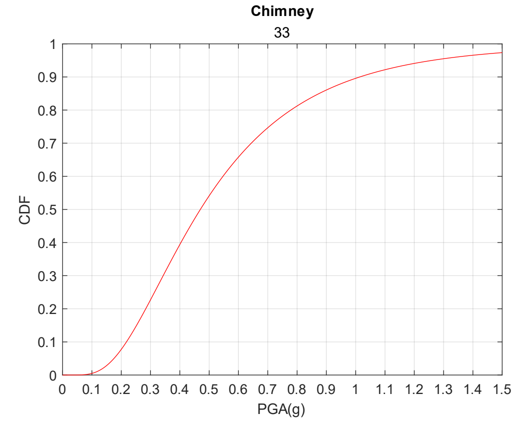

This Paper Fragility Curve

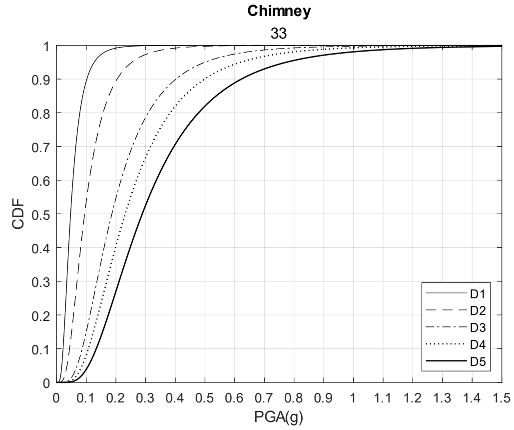

Chimney Number	34
X	146.624
Y	-37.627
Z	320.803
Relative Mortar Condition	Medium
Damage State	No Damage
D – Level	2

Image

Maison and McDonald (2018) Fragility Curve

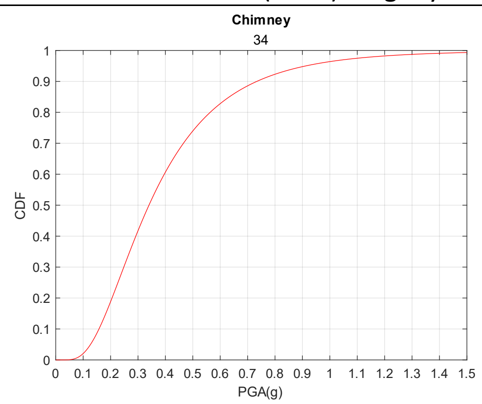

This Paper Fragility Curve

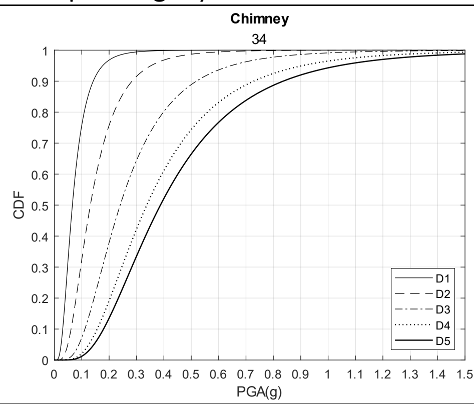

Chimney Number	35
X	146.6239
Y	-37.6271
Z	204.894
Relative Mortar Condition	Medium
Damage State	No Damage
D – Level	2

Image

Maison and McDonald (2018) Fragility Curve

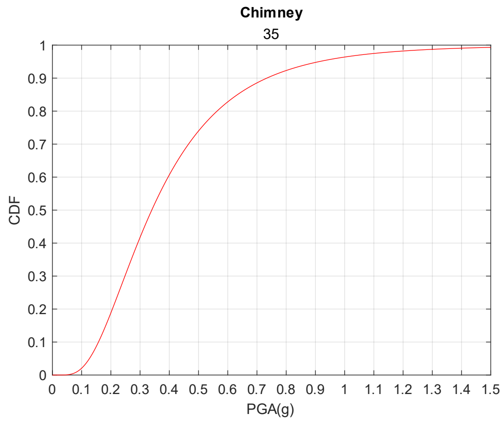

This Paper Fragility Curve

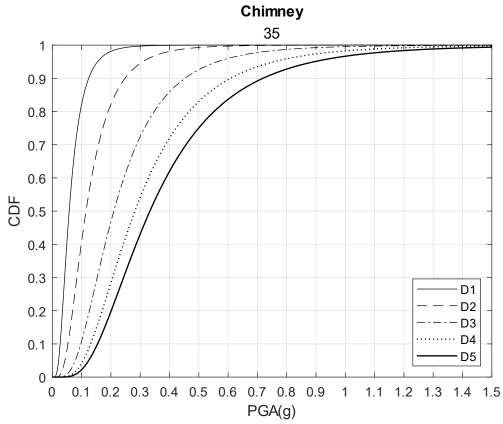

Chimney Number	36
X	146.6211
Y	-37.6292
Z	202.074
Relative Mortar Condition	Medium
Damage State	Collapse
D – Level	5

Image

Maison and McDonald (2018) Fragility Curve

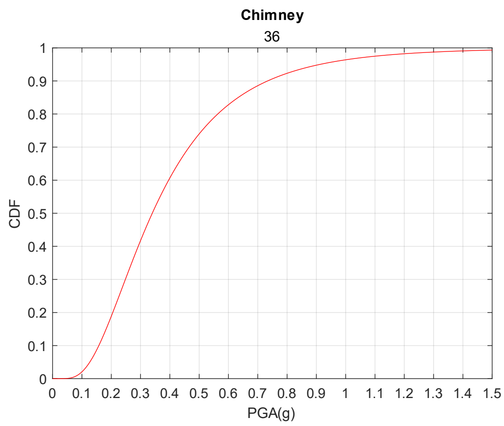

This Paper Fragility Curve

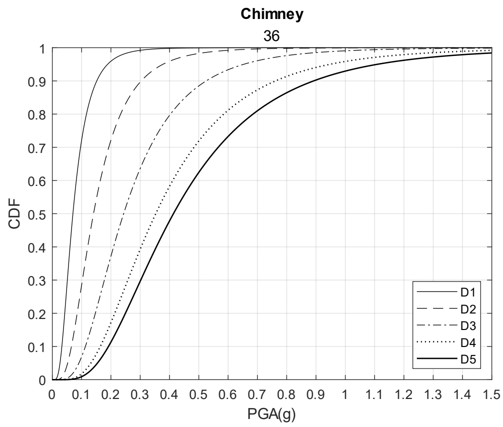

Chimney Number	37	Image
X	146.6156	
Y	-37.5171	
Z	323.214	
Relative Mortar Condition	Medium	
Damage State	No Damage	
D – Level	2	

Maison and McDonald (2018) Fragility Curve	This Paper Fragility Curve
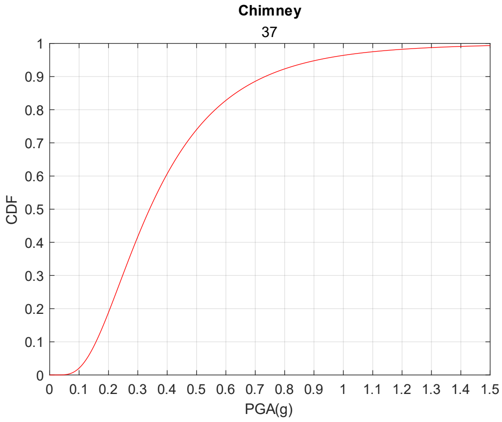	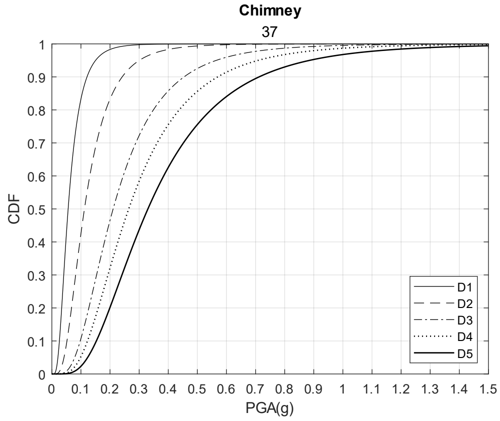

Chimney Number	38	Image
X	146.6155	
Y	-37.517	
Z	333.906	
Relative Mortar Condition	Medium	
Damage State	No Damage	
D – Level	2	

Maison and McDonald (2018) Fragility Curve	This Paper Fragility Curve
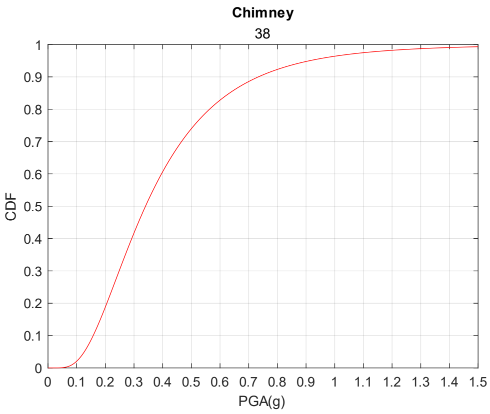	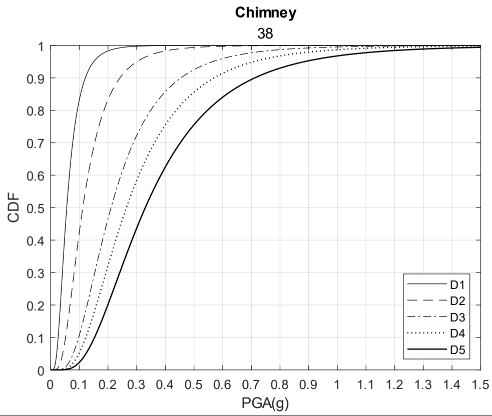

Chimney Number	39
X	146.5828
Y	-37.5896
Z	416.273
Relative Mortar Condition	Medium
Damage State	No Damage
D – Level	2

Image

Maison and McDonald (2018) Fragility Curve

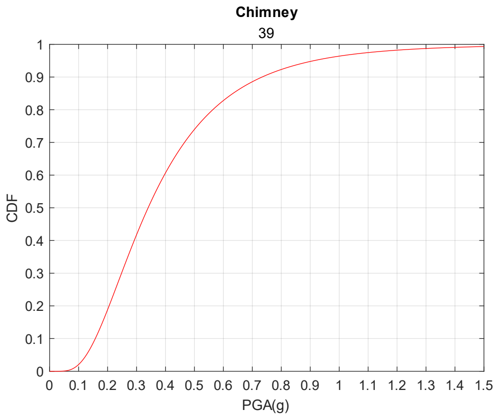

This Paper Fragility Curve

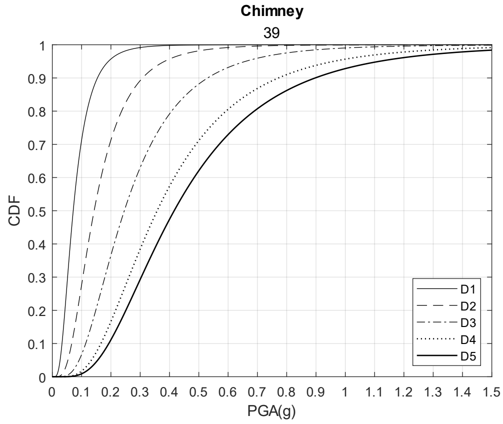

Chimney Number	40
X	146.5485
Y	-37.5143
Z	436.537
Relative Mortar Condition	Medium
Damage State	Collapse
D – Level	5

Image

Maison and McDonald (2018) Fragility Curve

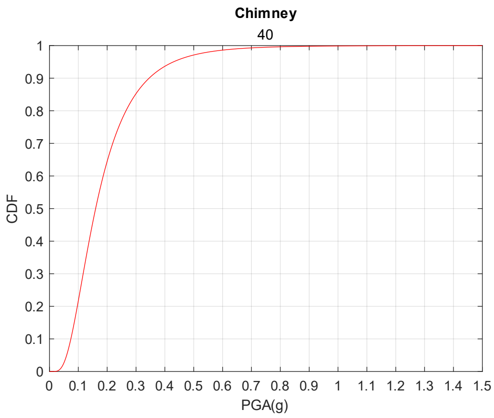

This Paper Fragility Curve

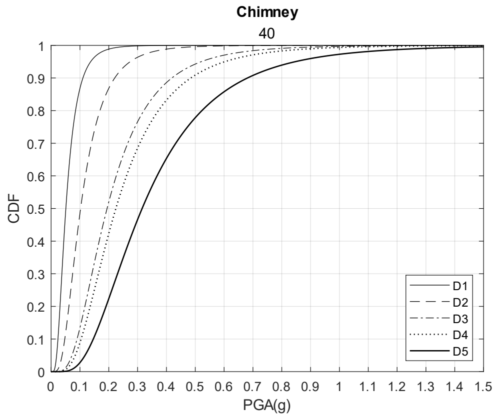

Chimney Number	41	Image
X	146.547	
Y	-37.5282	
Z	386.592	
Relative Mortar Condition	Good	
Damage State	No Damage	
D – Level	2	

Maison and McDonald (2018) Fragility Curve	This Paper Fragility Curve
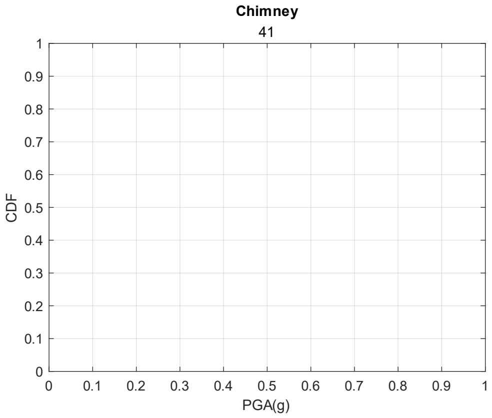	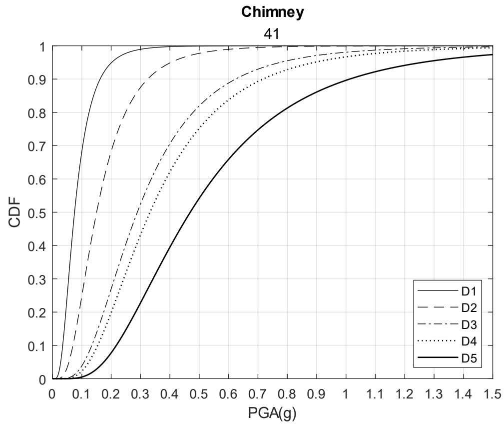

Chimney Number	42	Image
X	146.7107	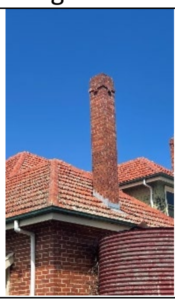
Y	-38.0158	
Z	52.9795	
Relative Mortar Condition	Medium	
Damage State	No Damage	
D – Level	2	

Maison and McDonald (2018) Fragility Curve	This Paper Fragility Curve
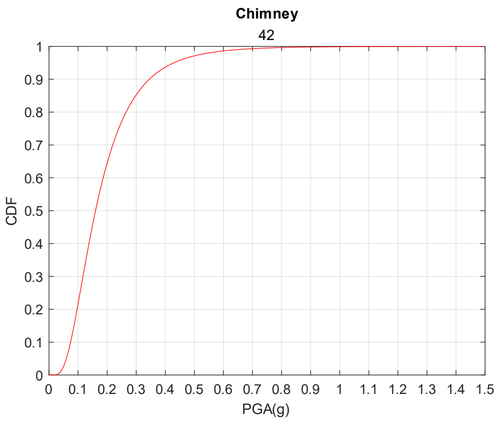	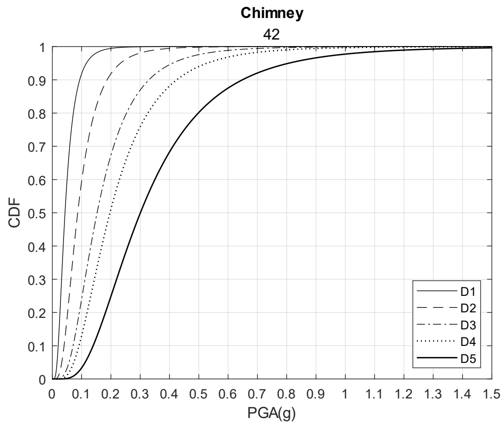

Chimney Number	43	Image
X	146.7107	
Y	-38.0158	
Z	52.9795	
Relative Mortar Condition	Medium	
Damage State	No Damage	
D – Level	2	

Maison and McDonald (2018) Fragility Curve	This Paper Fragility Curve
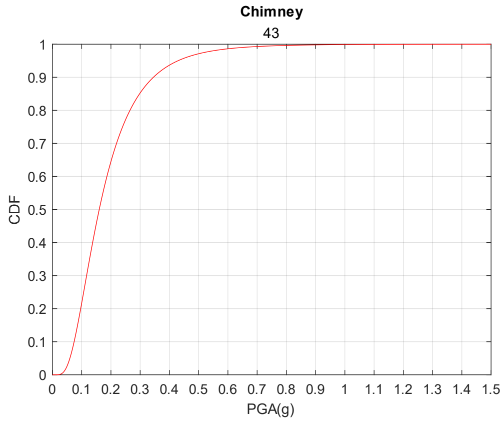	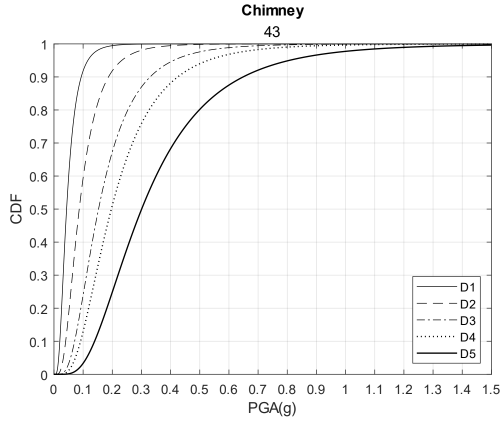

Chimney Number	44	Image
X	146.7107	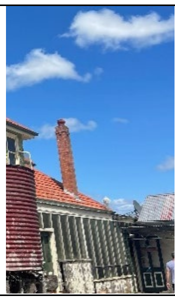
Y	-38.0158	
Z	52.9795	
Relative Mortar Condition	Medium	
Damage State	No Damage	
D – Level	2	

Maison and McDonald (2018) Fragility Curve	This Paper Fragility Curve
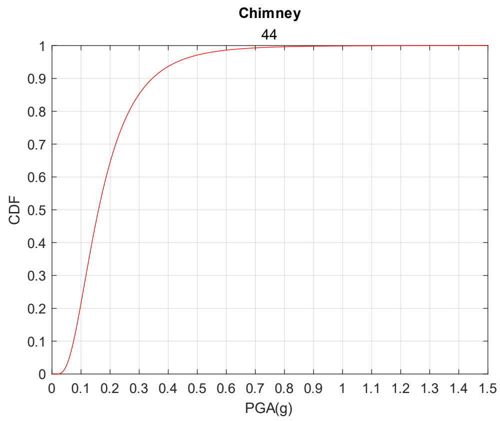	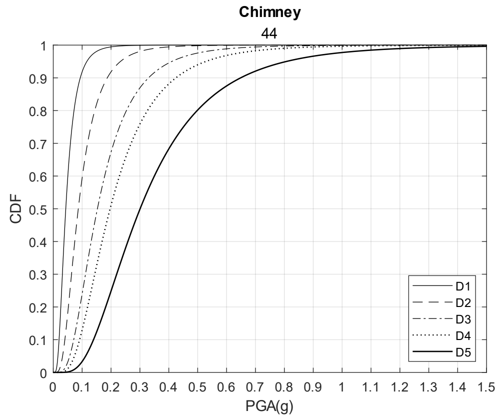

Chimney Number	45	Image
X	146.7107	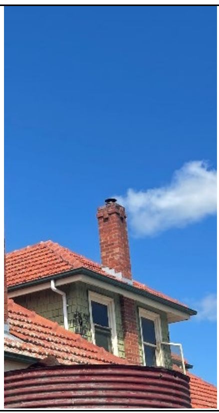
Y	-38.0158	
Z	52.9795	
Relative Mortar Condition	Medium	
Damage State	No Damage	
D – Level	2	

Maison and McDonald (2018) Fragility Curve	This Paper Fragility Curve
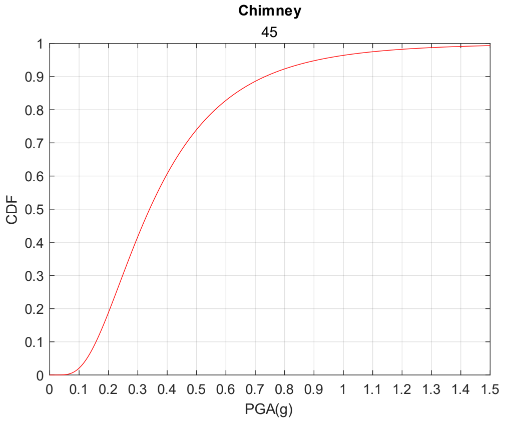	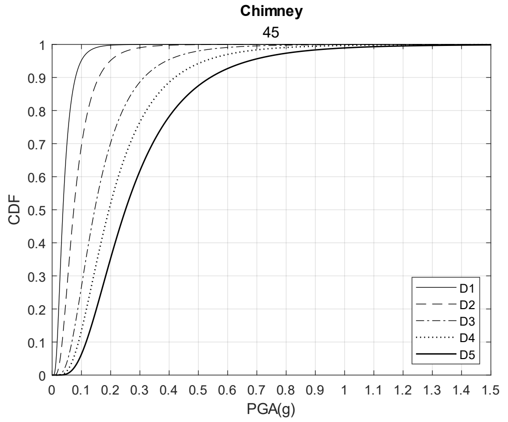

Chimney Number	46	Image
X	146.7107	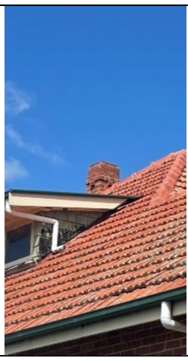
Y	-38.0158	
Z	52.9795	
Relative Mortar Condition	Medium	
Damage State	No Damage	
D – Level	2	

Maison and McDonald (2018) Fragility Curve	This Paper Fragility Curve
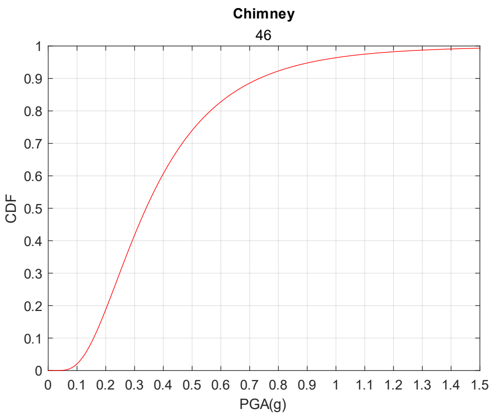	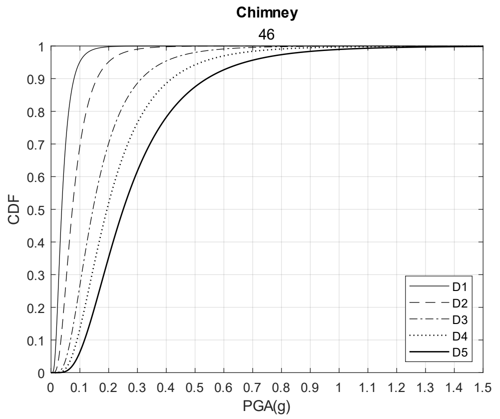

<table>
<tr><td>Chimney Number</td><td>47</td><td>Image</td></tr>
<tr><td>X</td><td>146.7107</td><td rowspan="6">No Image</td></tr>
<tr><td>Y</td><td>-38.0158</td></tr>
<tr><td>Z</td><td>52.9795</td></tr>
<tr><td>Relative Mortar Condition</td><td>Medium</td></tr>
<tr><td>Damage State</td><td>No Damage</td></tr>
<tr><td>D – Level</td><td>2</td></tr>
<tr><td colspan="2">Maison and McDonald (2018) Fragility Curve</td><td>This Paper Fragility Curve</td></tr>
<tr><td colspan="2">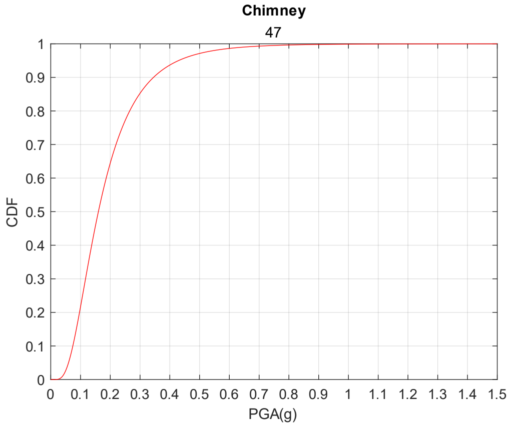
</td><td>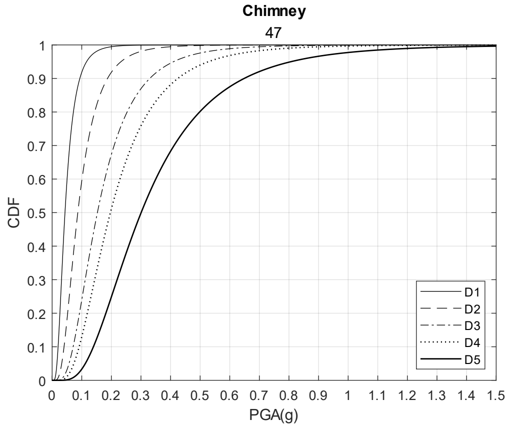
</td></tr>
</table>

Appendix B: Chimney inputs for fragility curve generation

Chimney Number	Brick A	Brick B	A (mm)	B (mm)	H (mm)	Type	No. Stories	Hb (mm)	Material	Relative Mortar Condition
1	2	2.5	460	575	1596	Building	1	4788	Brick	Medium
2	2	2.5	460	575	1900	Building	1	4750	Brick	Medium
3	2	2.5	460	575	1900	Building	1	4750	Brick	Medium
4	2.5	3.5	575	805	1140	Building	1	4700	Brick	Weak
5	2	2	460	460	3116	Ground			Brick	Weak
6			230	230	1976	Ground			Brick	Weak
7	2	2.5	460	575	1824	Building	1	3700	Brick	Medium
8	2.5	3	575	690	2356	Ground			Brick	Weak
9	2.5	3	575	690	2356	Ground			Brick	Weak
10			1000	1000	1000	Ground			Rubble	Extremely Poor
11			800	2109	1273	Ground			Rubble	Extremely Poor
12	2	2.5	460	575	1748	Ground			Brick	Weak
13	2	2	460	460	1444	Building	1	3249	Brick	Medium
14	2	2	460	460	1444	Building	1	3249	Brick	Medium
15	2	3.5	460	805	836	Building	1	6000	Brick	Medium
16	2	2	460	460	304	Ground			Brick	Weak
17	2	2.5	460	575	684	Building	1	4700	Brick	Weak
18	2	2	460	460	1520	Building	1	3700	Brick	Medium
19	2	2	460	460	1520	Building	1	3700	Brick	Medium
20	2.5	4	575	920	570	Building	1	3300	Brick	Medium
21			1000	1850	3373	Ground			Rubble	Extremely Poor
22			1000	1000	1000	Ground			Rubble	Extremely Poor
23	2	2.5	460	575	1596	Ground			Brick	Weak
24	2	2.5	460	575	608	Ground			Brick	Weak
25	6	2	1380	460	912	Building	1	3700	Brick	Weak
26	2	3	460	690	836	Building	1	3500	Brick	Weak
27	2.5	2.5	575	575	1596	Building	1	3700	Brick	Medium
28	2	2	460	460	1520	Building	1	2812	Brick	Weak
29	2	2	460	460	988	Building	1	2812	Brick	Weak
30	3.5	3.5	805	805	2280	Ground			Brick	Medium
31	2	2.5	460	575	760	Ground			Brick	Weak
32	2.5	3	575	690	3648	Building	1	3700	Brick	Good
33	2	2.5	460	575	1672	Building	1	6688	Brick	Good
34	2	5.5	460	1265	1064	Building	1	3344	Brick	Medium
35	2	5.5	460	1265	1444	Building	1	3344	Brick	Medium
36	2	3	460	690	912	Building	1	3700	Brick	Medium
37	2	2.5	460	575	1672	Ground			Brick	Medium
38	2	2.5	460	575	1672	Ground			Brick	Medium
39	2	6	460	1380	912	Building	1	3400	Brick	Medium
40	2	2.5	460	575	2128	Building	1	3700	Brick	Medium
41	3	4.5	690	1035	2128	Building	1	4300	Brick	Good
42	2	2	460	460	3192	Building	1	3344	Brick	Medium
43	2	2	460	460	3192	Building	1	3344	Brick	Medium
44	2	2	460	460	3192	Building	1	3344	Brick	Medium
45	2	2	460	460	1596	Building	2	5016	Brick	Medium
46	2	2	460	460	1596	Building	2	5016	Brick	Medium
47	2	2	460	460	3192	Building	1	3344	Brick	Medium

Appendix C:

Table 2: M1: Maison and McDonald (2018) median values for fragility curves.

Chimney Number	Median PGA
1	0.34
2	0.34
3	0.34
4	0.508
5	0.11
6	
7	0.34
8	0.123
9	0.123
10	
11	
12	0.135
13	0.34
14	0.34
15	
16	0.44
17	0.44
18	0.34
19	0.34
20	
21	
22	
23	0.135
24	0.44
25	0.44
26	0.44
27	0.41
28	0.135
29	0.135
30	
31	
32	0.23
33	0.47
34	0.34
35	0.34
36	0.34
37	0.34
38	0.34
39	0.34
40	0.16
41	
42	0.16
43	0.16

44	0.16
45	0.34
46	0.34
47	0.16

Table 2: M2 Median Values for fragility Curves.

Chimney Number	median PGA (g)				
	D1	D2	D3	D4	D5
1	0.05	0.10	0.20	0.26	0.31
2	0.05	0.10	0.20	0.23	0.31
3	0.05	0.10	0.20	0.23	0.31
4	0.07	0.15	0.28	0.39	0.43
5	0.05	0.09	0.16	0.20	0.31
6	0.03	0.05	0.10	0.12	0.17
7	0.05	0.10	0.20	0.24	0.32
8	0.07	0.13	0.24	0.27	0.40
9	0.07	0.13	0.24	0.27	0.40
10	0.16	0.32	0.57	0.80	0.90
11	0.11	0.22	0.40	0.55	0.63
12	0.06	0.11	0.21	0.26	0.33
13	0.06	0.12	0.21	0.28	0.33
14	0.06	0.12	0.21	0.28	0.33
15	0.06	0.13	0.22	0.33	0.38
16	0.23	0.46	0.69	0.65	0.69
17	0.08	0.17	0.26	0.37	0.45
18	0.05	0.11	0.20	0.27	0.32
19	0.05	0.11	0.20	0.27	0.32
20	0.13	0.26	0.40	0.51	0.65
21	0.09	0.19	0.33	0.44	0.66
22	0.16	0.32	0.57	0.80	0.90
23	0.06	0.11	0.21	0.27	0.33
24	0.11	0.23	0.34	0.43	0.55
25	0.07	0.14	0.24	0.35	0.41
26	0.08	0.15	0.25	0.37	0.43
27	0.07	0.13	0.25	0.33	0.39
28	0.06	0.11	0.21	0.27	0.33
29	0.07	0.14	0.25	0.35	0.40
30	0.09	0.19	0.34	0.39	0.56
31	0.09	0.19	0.28	0.41	0.48
32	0.05	0.10	0.18	0.25	0.37
33	0.05	0.09	0.19	0.23	0.29
34	0.07	0.13	0.24	0.34	0.39
35	0.06	0.12	0.21	0.28	0.33
36	0.07	0.14	0.24	0.35	0.41
37	0.06	0.11	0.21	0.26	0.33
38	0.06	0.11	0.21	0.26	0.33

39	0.07	0.14	0.25	0.36	0.42
40	0.05	0.10	0.19	0.22	0.32
41	0.08	0.15	0.29	0.33	0.47
42	0.04	0.09	0.15	0.20	0.30
43	0.04	0.09	0.15	0.20	0.30
44	0.04	0.09	0.15	0.20	0.30
45	0.04	0.07	0.15	0.19	0.25
46	0.04	0.07	0.15	0.19	0.25
47	0.04	0.09	0.15	0.20	0.30

Appendix D

Appendix D is supplementary material in the form of an excel spread sheet. Please see the attached drop box link.

https://www.dropbox.com/s/0wfg36r5cldfkk8/Appendix%20G.xlsx?dl=0